ELSEVIER

Polymer 40 (1999) 6235–6263

polymer

A phenomenological study of the hot-tool welding of thermoplastics. Part 1: Polycarbonate ☆

Vijay K. Stokes

GE Corporate Research and Development, Engineering Mechanics Laboratory, P.O. Box 8, Schenectady, NY 12301, USA

Received 5 January 1998; received in revised form 20 May 1998; accepted 12 August 1998

Abstract

A dual platen hot-tool welding machine, in which the temperatures of the two hot-tool surfaces can be independently controlled, was used to study the weldability of bisphenol-A polycarbonate. In these experiments, the outflow in the melting phase was controlled by means of stops, the thickness of the molten film was controlled by the heating time, and the outflow during the final joining phase was also controlled by displacement stops. Strength data for butt welds are reported for a series of tests — both on dried and undried specimens — in which the hot-tool surface temperatures, the heating times, and the displacement stop positions were varied, but the pressure was not. Weld strength data are reported for three specimen thicknesses. It is shown that very high weld strengths can be achieved, even in the undried material.

Keywords: Hot-tool welding; Thermoplastics; Bisphenol-A polycarbonate

1. Introduction

Because of the increasing use of thermoplastics and thermoplastic composites in load-bearing applications, welding methods are becoming important for part cost reduction. Welding requires the melting of the surfaces to be joined, followed by a solidification of the interfacial molten layers under pressure. One widely used technique is hot-tool welding, in which the surfaces to be joined are brought to the ''melting temperature'' by direct contact with a heated metallic tool. In some cases, such as joining of plastic pipes, the surfaces to be joined are flat, so that the tool is a hot plate. However, in many applications, such as in automotive headlamps and rear lights, doubly curved joint interfaces require complex tools that allow the hot surfaces to match the contours of the joint interface. Applicability to complex geometries is one of the major advantages of this process.

This paper examines the hot-tool weldability of bisphenol-A polycarbonate (PC). A dual platen hot-tool welding machine, in which the temperatures of the two hot-tool surfaces can be independently controlled, was used to study the weldability of polycarbonate. In these experiments, the outflow in the melting phase was controlled by means of stops, the thickness of the molten film was controlled by the heating time, and the outflow during the final joining phase was also controlled by displacement stops. Strength data for butt welds are reported for a series of tests — both on dried and undried specimens — in which the hot-tool surface temperatures, the heating times, and the displacement stop positions were varied, but the pressure was not. The effects of the large number of welding parameters were explored mainly by conducting one test per test condition studied. Such data do not provide information on the variability in the weld strength at each test condition. The variability in the data was then studied through repeat tests at the near optimum conditions established by the single tests. It is shown that very high weld strengths can be achieved, even in the undried material.

The hot-tool welding process can be described in terms of the four phases schematically shown by the pressure–time diagram in Fig. 1 [1]. In phase 1, the parts are brought into contact with the hot-tool, and a relatively high pressure is used to ensure complete matching of the part and tool surfaces. The pressure is maintained until the molten plastic begins to flow out laterally. In phase 2, the melt pressure is reduced to allow the molten film to thicken. The rate at which the film thickens is controlled by heat conduction through the molten layer. When a sufficient molten film thickness has been achieved, the part and tool are separated. This third phase is referred to as the changeover phase; its

☆ Based on a paper presented at the Society of Plastics Engineers 53rd Annual Technical Conference, 7–11 May 1995, Boston, MA, USA.

0032-3861/99/$ - see front matter
PII: S0032-3861(98)00584-9

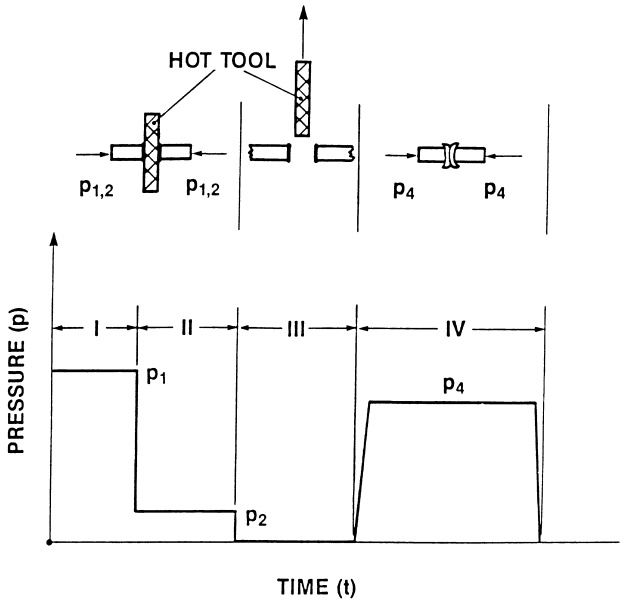

Fig. 1. Schematic pressure–time graph showing the four phases of the hot-tool welding process (adapted from Ref. [2]).

duration should be kept to a minimum to prevent premature cooling of the molten film. The molten interfaces of the parts to be joined are then brought together and held under pressure until the weld solidifies. During this final joining phase the molten material flows laterally outward, while undergoing cooling and solidification. Clearly, the important welding parameters for this process are the hot-tool temperatures during phases 1 and 2, the matching pressure during phase 1, the melt pressure during phase 2, the changeover time, the separation and rejoining velocities, and the weld pressure and duration of phase 4. This hot-tool welding technique — commonly referred to as welding by pressure — requires machines in which the applied pressure can be accurately controlled. One shortcoming of this process is that the final part dimensions are not controlled directly. In particular, variations in the part-to-part film thickness and the sensitivity of the melt viscosities of thermoplastics to small temperature changes can result in unacceptable variations in part dimensions.

A modification of the method discussed above, called welding by distance, uses rigid stops to control the process and part dimensions. As in welding by pressure, the parts to be joined are first forced against the hot-tool, but the

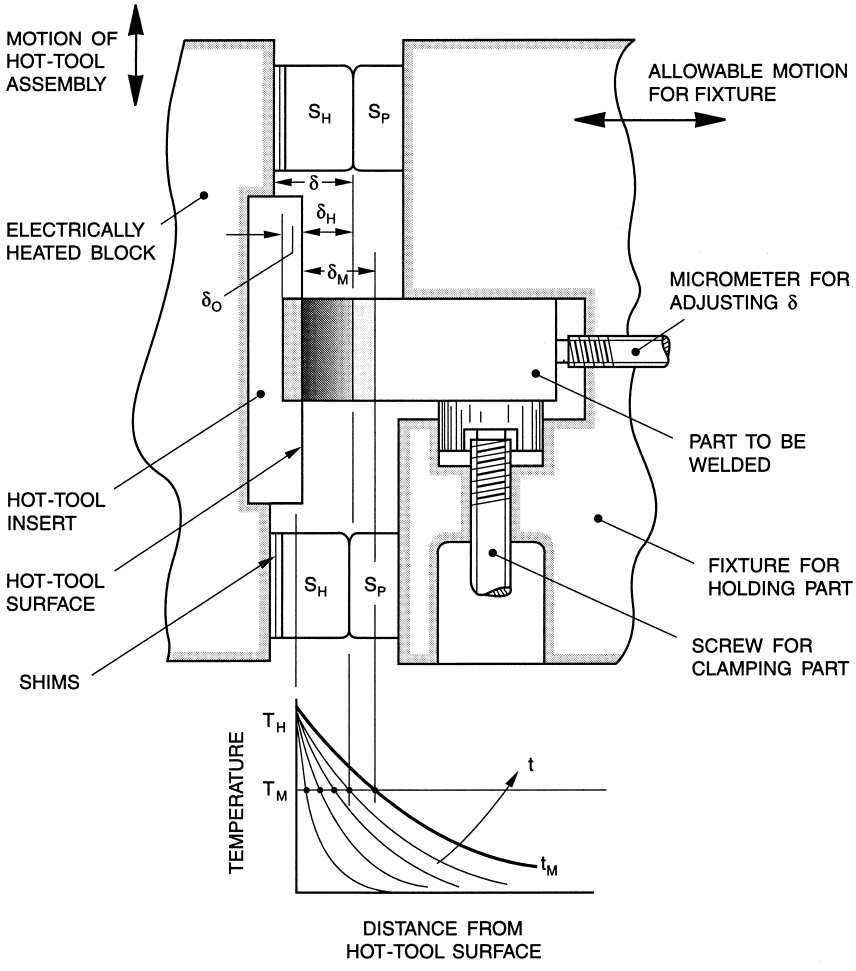

Fig. 2. Schematic diagram showing geometric parameters for displacement-controlled hot-tool welding using mechanical stops.

displacements of the parts during phase 1 are restricted to predetermined distances by means of mechanical stops. In phase 2, the parts are held in place against the stops for a predetermined time to allow the molten layer to thicken. During the final joining phase, mechanical stops are again used to inhibit the motion of the parts, thereby allowing the molten film to solidify solely by heat conduction, without any gross flow. In this way part dimensions can be controlled more accurately. However, computer controlled machines, in which pressure or displacement can be programed over different phases of the welding cycle, are now available [2].

Although considerable progress has been made in experimentally characterizing hot-tool welding [3–12], the underlying process physics was analyzed in terms of highly simplified models [2,13–16]. For example, these models assume that the melt viscosity is constant during the final joining phase. Because the viscosity of a polymer melt can decrease by more than a factor of two for a 10°C increase in temperature, any realistic model for the welding process must account for this effect [17]. A more recent analysis of the hot-tool welding process [18] has shown that this temperature sensitivity has a dramatic effect on the process conditions within the molten layer. That analysis has also shown how the use of stops affects the welding process.

In principle, any polymer that melts on heating can be welded by the hot-tool welding process. By using different hot-tool temperatures for the two parts of an assembly, it should be possible to weld dissimilar materials [19,20]. The literature on the welding of dissimilar materials is quite small. The few papers on hot-tool welding are mainly concerned with the weldability of different grades of HDPE [21,22] and the welding of PP homopolymer to a PP copolymer [23]. Ref. [24] discusses the hot-tool welding of polycarbonate, poly(butylene terephthalate), and polyetherimide to each other. Certainly, the welding of dissimilar materials has not been explored systematically; nor have process models been developed.

2. Displacement controlled welding

The essential parts of such a welding machine consist of the hot-tool assembly having two exposed hot surfaces, two fixtures for holding the parts to be welded, means for bringing the parts in contact with the hot surfaces and then bringing the molten surfaces together to form the weld, and adequate timing and displacement controls. The mechanics of the hot-tool welding process using mechanical stops to effect displacement control can be described by means of the schematic in Fig. 2. The left-hand side of this figure shows one-half of the hot-tool assembly, comprising an electrically heated block on which interchangeable hot-tool inserts (in this case a flat insert) can be mounted. Normally, a single hot-tool that has two exposed hot surfaces is used for heating the two parts of an assembly, especially for flat-surfaced parts made of the same material. However, in dual platen hot-tool machines the two halves can be independently heated to maintain the two exposed surfaces at different temperatures. The hot-tool assembly has mechanical stops S_H, the surfaces of which are offset from the hot-tool surface by a distance δ_H. The hot-tool assembly can be moved in and out of the configuration shown in the figure along the direction indicated.

The part to be welded is gripped in a fixture (right-hand side of Fig. 2) that can be moved to and fro in a direction at right angles to the allowable motion for the hot-tool assembly. This fixture has mechanical stops S_P that are aligned with the hot-tool stops S_H. Let the distance by which the part surface protrudes beyond the surfaces of the stops S_P be $\delta = \delta_0 + \delta_H$, as shown in the figure.

For welding, the hot-tool assembly is first moved into the position shown. Then the part fixture is moved in the direction indicated to bring the part into contact with the hot-tool surface, and a pressure is applied to maintain this contact. (Clearly, contact is possible only when $\delta \geq \delta_H$.) Heat transfer raises the temperature of the part and the resulting thermal expansion causes a small rightward (away from the hot-tool surface) motion in the part and fixture. When the surface temperature reaches the melting point of the plastic the part surface begins to melt. The externally applied pressure causes the molten material to flow laterally outward, thereby inducing a leftward motion of the part. The decrease in the part length caused by the outflow of molten material will be called the penetration η, which for this phase will be the part displacement from the instant of contact, and weld time will be measured from this instant of contact.

Initially, when the surface begins to melt, there will be very little flow and the molten film will thicken. The flow or penetration rate will begin to increase with time, eventually reaching a steady state at which the rate of outflow equals the rate at which the material is melting; from this point on the penetration will increase linearly with time [17]. However, when stops are used, the penetration (or part motion) will not change after the part stops S_P come into contact with the hot-tool stops S_H, as shown in Fig. 2 [18]. (Of course, stop contact can occur before the steady-state is attained.) Let the elapsed time from the instant that the part touches the hot-tool surface to the instant when the stops come into contact be t_0, and let the corresponding penetration be $\eta = \delta_0$ (Fig. 2).

This thickness of material will melt and flow out laterally to form a part of the weld ‘‘bead’’. Continuing contact with the hot-tool surface after time t_0 will cause the molten layer to thicken with time. During this phase there will be no additional penetration. However, thermal expansion in the portion of the part heated by conduction will cause more material to flow out with increasing time, thereby resulting in an apparent increase in δ_0. Let the duration of this film buildup phase be t_M and let the thickness of the molten layer be δ_M as shown. The melt/solid interface can be defined as the surface in the material that has attained the ‘‘melting’’

temperature T_M. In the changeover phase, the parts are pulled away from the hot-tool, the hot-tool is retracted, and the molten surfaces are brought into contact — thereby initiating the joining phase. Let the duration of this changeover phase, which should be as small as possible, be t_c. After the molten surfaces touch, the applied joining pressure squeezes out the molten material laterally, resulting in a further penetration. During this squeezing motion, heat transfer from the melt results in a cooling and in an eventual solidification of the melt.

Two possible cases are important. If $\delta_M < \delta_H$, the part stops S_P cannot come into contact, so that part dimensions cannot be controlled. However, if $\delta_M > \delta_H$ the material in the molten layer will continue to be squeezed out until the stops S_P come into contact, after which part motion will stop and the melt will solidify without further motion. Of course, even when $\delta_M > \delta_H$, the stops may not contact if the imposed joining penetration rate is artificially low, so that the material freezes before the stops contact. However, this case is not of practical importance because the joining penetration rate is high. Thus, for dimensional control t_M should be large enough to ensure that $\delta_M > \delta_H$. For this case, the total penetration on each of the halves being welded will be $\delta = \delta_0 + \delta_H$, so that the overall (warm) part length will decrease by 2δ, if thermal expansion effects are neglected. Let the initial lengths of the parts before welding be l_1 and l_2, and let the length of the welded part be l_0. Then, $\Delta l = l_1 + l_2 - l_0$ is the thickness of the material that flowed out into the weld bead. If the stops come into contact during the joining phase (for which $\delta_M > \delta_H$) and thermal expansion effects are neglected, then the expected change in length should be 2δ. However, if $\delta_M < \delta_H$, then the stops will not come into contact and the change in length should be less than 2δ. Thus, *if* thermal expansion effects are neglected, $\Delta\eta = 2\delta - \Delta l$ is a measure for whether or not the stops come into contact: stops do and do not contact when $\Delta\eta = 0$ and $\Delta\eta > 0$, respectively. However, thermal expansion at the heated ends of the specimens would increase Δl and, in the case in which stops contact, could result in negative values of the differential penetration $\Delta\eta$. Thus, a larger Δl could result from thermal expansions both in Phase 1 (an apparent increase in δ_0) and during the joining phase. Let the thermal expansion of the specimen be δ_T, so that the effective change in length would be $2(\delta + \delta_T)$. Then, $\Delta\eta_T = 2(\delta + \delta_T) - \Delta l$ will be a better measure for whether or not stops come into contact.

As the molten material cools, thermal contraction generates tensile stress in the solidifying material. This stress field can affect the residual stresses induced by the nonhomogeneous cooling. Clearly, δ_0 by itself does not contribute to the welding that occurs during the joining phase — this thickness of material just flows outward into the bead. A small value of δ_0 is required to compensate for part surface irregularities and for ensuring that contaminated surface layers flow out before the joining phase. The penetration $\eta_j = \delta_H$ during the joining phase is controlled by the machine setting δ_H (Fig. 2). Let the duration of the joining (or welding) phase, from the instant the molten surfaces touch to the instant the solidified weld is released, be t_w. Then the total welding time is given by $t_T = t_0 + t_M + t_c + t_w$. Clearly, t_c should be as small as possible.

2.1. Estimates for thermal expansion effects

As the temperature of the specimen in contact with the hot-tool surface increases, thermal expansion will cause its length to increase. A determination of this length change first requires a calculation of the temperature distribution. In the real problem, the material surface exposed to the hot-tool will change with time because of lateral flow of the molten material. However, the extent of this outflow will be limited by the stops. To simplify the problem, it will be assumed that the hot-tool remains in contact with the same material surface on the specimen, without any lateral flow. Let the x coordinate be measured into the specimen with the hot-tool specimen surface being at $x = 0$. Then, if the thermal diffusivity κ is assumed constant, the temperature distribution in the specimen will be given by $T(x,\ t) - T_a = (T_H - T_a)\ \mathrm{erfc}(x/\sqrt{4\kappa t})$, where T_a is the initial (ambient) temperature of the specimen [25]. The thermal strain is then given by

$$\varepsilon_T(x,\ t) = \alpha\,(T_H - T_a)\ \mathrm{erfc}(x/\sqrt{4\kappa t})$$

An integration of $\mathrm{d}u/\mathrm{d}x = \varepsilon_T(x,\ t)$, where u is the displacement, then determines the temperature-induced increase in the specimen length δ_T as

$$\begin{aligned}\delta_T &= \int_0^\infty \alpha\,(T_H - T_a)\ \mathrm{erfc}\left(x/\sqrt{4\kappa t}\right)\mathrm{d}x \\ &= \alpha\,(T_H - T_a)\sqrt{4\kappa t}\int_0^\infty \mathrm{erfc}(\xi)\,\mathrm{d}\xi \\ &= \alpha\,(T_H - T_a)\sqrt{4\kappa t}\ \mathrm{ierfc}(0) = \frac{2\alpha}{\sqrt{\pi}}(T_H - T_a)\sqrt{\kappa t} \qquad (1)\end{aligned}$$

where the thermal expansion coefficient α has been assumed constant (temperature independent).

Thus, by assuming no melt outflow at the hot-tool surface, and by further assuming that the thermal diffusivity and the thermal expansion coefficients are temperature-independent, an estimate for the thermal expansion of the specimen is given by Eq. (1). This constant-property approximation requires representative values for κ and α. The thermal diffusivity of PC varies from $0.172\ \mathrm{mm^2\,s^{-1}}$ at 20°C to $0.099\ \mathrm{mm^2\,s^{-1}}$ at 150°C. The thermal expansion coefficient of PC decreases continuously from $6.4\times10^{-5}(°C)^{-1}$ at 20°C to $6.2\times10^{-5}\ (°C)^{-1}$ at 140°C. It undergoes a large change near the glass transition temperature, $T_g = 155$°C, of PC. Above T_g, α varies from $2.2\times10^{-4}\ (°C)^{-1}$ at 155°C to $2.0\times10^{-4}\ (°C)^{-1}$ at 275°C, to $1.9\times10^{-4}\ (°C)^{-1}$ at 350°C to $1.9\times10^{-4}\ (°C)^{-1}$ at 410°C. One approach for estimating the thermal expansion would be to integrate the first expression in Eq. (1) using a step function for α, with $\alpha =$

Table 1
Estimates for thermally induced length increases in PC specimens at different hot-tool temperatures and heating times, for an ambient temperature of $T_a = 20$°C

Hot-tool temperature (°C)	Estimate for thermally induced expansion δ_T (10^{-2} mm)				
	$t_H = 5$ s	$t_H = 10$ s	$t_H = 15$ s	$t_H = 20$ s	$t_H = 30$ s
200	3	4	5	6	7
215	3	4	5	6	8
230	3	5	6	7	8
245	4	5	6	7	9
260	4	5	7	8	9
275	4	6	7	8	10
290	4	6	7	9	11
305	5	6	8	9	11
320	5	7	8	9	12
335	5	7	9	10	12
350	5	7	9	11	13
365	6	8	10	11	13
380	6	8	10	11	14
395	6	8	10	12	15
410	6	9	11	12	15
425	6	9	11	13	16

6×10^{-5} (°C)$^{-1}$ for $T < 150$°C and $\alpha = 2 \times 10^{-4}$ (°C)$^{-1}$ for $T \geq 150$°C. However, since the focus here is on obtaining an *estimate* for δ_T, an upper bound for δ_T will be obtained by using a constant thermal expansion coefficient of $\alpha = 2 \times 10^{-4}$ (°C)$^{-1}$. By assuming a constant κ of 0.1 mm^2 s^{-1}, the expression in Eq. (1) then reduces to $\delta_T = 0.714 \times 10^{-4}(T_H - T_a)\sqrt{t}$ mm. From this expression, estimates for δ_T at different hot-tool temperatures and heating times, for an ambient temperature of $T_a = 20$°C, are listed in Table 1.

3. Test procedure

All the test data in this paper were obtained from specimens cut from 3-, 5.8-, and 12-mm-thick extruded sheets of bisphenol-A polycarbonate (LEXAN® 9030). The edges of each specimen were machined to obtain rectangular blocks of size 76.2 × 25.4 mm × thickness for assuring accurate alignment of the surfaces during butt welding along the 25.4 mm × thickness edges. Tests were done both on undried (equilibrated at an ambient condition of 22°C and 50% relative humidity) and dried specimens. (The specimens were dried in an oven for 24 h at a temperature of 127°C.)

All the welds were made on a commercially available (Hydra-Sealer Model VA-1015, Forward Technology Industries, Inc.) dual platen hot-tool welding machine in which the temperatures of the two hot-tool surfaces can be independently controlled. On this machine, the offset δ_H, called the melt penetration, of the hot-tool stop S_H from the hot-tool surface (Fig. 2) can only be changed by inserting shims between the electrically heated hot-tool block and the stops, which are fastened to the block surface by means of screws. Most of the data in this paper were obtained at two melt penetrations of $\delta_H = 0.25$ and 0.66 mm.

The weld specimens are pneumatically gripped in special fixtures that accurately align the specimens during the welding cycle. Each grip is provided with a micrometer that can be used to accurately set the distance δ by which each specimen protrudes beyond the stops S_P, any variations in the lengths of the specimens can easily be compensated for. In this machine, the times t_0 and t_M cannot be resolved — only the total heating time $t_H = t_0 + t_M$ can be set and measured. However, for $\delta_0 \ll \delta_H$, t_0 should be much smaller than t_M. The changeover time t_c, from the instant the heated specimens are pulled back from the hot-tool to the instant the molten films are brought back into contact, can be changed by changing the decelerating springs and the air pressure on the displacement pistons. However, the possible range of variation is quite small. In the tests reported in this paper, a fixed changeover time t_c of about 1.24 s was used; the corresponding average changeover velocity seen by the specimen molten surfaces was about 118 mm s^{-1}. The welding, or joining time, t_w, measured from the instant the molten films are brought into contact to the instant the (solidified) welded parts are released, can be preset on this machine.

One major shortcoming of this machine is the lack of adequate pressure control at the weld interface. The specimens are loaded by air pressure acting on pistons that are used to generate the to and fro joining motion. Pressure times the piston cross-sectional area determines the axial load on the specimen, from which the interfacial weld pressure can be calculated. However, near the end of piston travel — when the specimens are about to contact the hot-tool surfaces or when the molten surfaces of the specimens are about to contact during the joining phase

— decelerating springs come into play to cushion the contact. As a result, the interfacial pressure during the initial part of the joining phase varies in a way that is a characteristic of the machine. While this variation is repeatable, it has not been characterized for this machine. For 3-, 5.5-, and 12-mm-thick PC welds (specimen cross sections of thickness × 25.4 mm), the nominal weld pressures (based on the air pressure and the piston cross-sectional area) were 7.4, 3.9, and 1.9 MPa, respectively.

An important characteristic of the hot-tool surface is the extent to which molten polymer tends to stick to the surface. Residue left behind can affect the quality of subsequent welds: First, because of the high temperature, the accumulated material can degrade, transfer to subsequent welds, and act as an inclusion. Second, the accumulated layer can affect heat transfer. And third, the texture of the surface residue can affect the geometry of the molten part surface. To reduce this tendency for sticking, the surface of the hot-tool insert can be coated with a non-stick coating, such as Teflon®; an example is provided by commonly used Teflon coated aluminum inserts. An alternative is to cover the hot-tool surface with a thin Teflon cloth — as it degrades or becomes coated, a fresh Teflon surface is made available by sliding the cloth over the hot-tool. However, Teflon coatings and cloth can only be used up to hot-tool temperatures of about $T_H = 260°C$. Because higher weld temperatures are required for PC, an uncoated metal insert, made of a high-conductivity copper–nickel–silicon–chromium alloy (Ampco 940, about 96% of which is copper), was used for all the tests reported in this paper. To eliminate the effects of residues resulting from the tendency of the melt to stick to the surface, a copper scraper was used to clean the hot-tool surface after each test.

The texture of the melt surface just before the final joining phase can be expected to affect weld quality. For example, any surface roughness could trap air during the joining phase. A series of tests was done to study the effects of the hot-tool temperature and the melt time on the texture of the molten surface. Undried and dried 5.8-mm-thick PC specimens — whose lengths had been accurately determined — were mounted in the left and right specimen holders, respectively. The micrometers were set to obtain melt penetrations of 0.13 mm on both specimens. After the specimens had been heated to the specified heating time (5, 10, 15, and 20 s), the specimens were retracted from the hot-tool surfaces and the weld cycle stopped. On cooling, the specimens were removed from the machine and the ''heated'' surfaces examined. The surfaces of the hot-tool were also examined after each test to check for residues and to determine the ease with which the hot-tool surfaces could be cleaned. Measurements of the final specimen lengths were used to determine changes in lengths. The test matrix consisted of 15 hot-tool temperature from 230°C to 440°C in steps of 15°C, with four heating times of 5, 10, 15, and 20 s at each hot-tool temperature, for a total of 60 tests.

The test procedure for determining weld strength is as follows: First, the hot-tool surfaces are allowed to attain the desired surface temperatures. After accurately measuring their lengths, the weld specimens are mounted on the specimen holding fixtures and the micrometer settings are adjusted to obtain desired values of the overhang δ. The heating time t_H and the welding time t_w are set and the machine is cycled to effect the weld. The weld results in a 152.4 × 25.4 mm × thickness bar. After sufficient cooling, the length of the bar is accurately measured with a micrometer. The difference Δl of this final length from the combined lengths of the unwelded specimen pairs determines the thickness of the material that actually flowed out, that is, the actual penetration, which can be compared with 2δ.

The rectangular bar is routed down to a standard ASTM D638 tensile test specimen with a butt joint at its center. The tensile bar, which has a transverse butt weld at mid-length, is then subjected to a constant displacement rate tensile test in which the strain across the weld is monitored with an extensometer. In this way the average failure strain across the weld over a 25.4-mm gauge length can be monitored. All the weld strength tensile tests reported in this paper were done at a nominal strain rate of 0.01 s^{-1}.

The weld flash, or ''bead'', was not removed, and the weld strengths were obtained by dividing the load at failure by the original cross-sectional area of the specimen. Because large local deformations at the weld interface increase the local cross-sectional area, the true failure stress (based on the actual local cross-sectional area) will be smaller than the nominal stress (based on the original cross-sectional area) reported in this paper [26].

Further, the 25.4-mm gauge-length extensometer can grossly underestimate the local strain in the failure region once strain localization sets in, so that the significance of the reported failure strains ϵ_0 should be interpreted with care. These values only represent the lower limit of the failure strain at the weld.

4. Molten surface texture

Air trapped between the surfaces to be joined just before the molten surfaces contact during the final joining phase can result in poor weld quality; therefore the texture of the molten surface is important. A series of 60 tests was done on undried and dried 5.8-mm-thick PC specimens to study the effects of the hot-tool temperature and the melt time on the texture of the molten surface. In these tests, specimens heated to the specified heating time were retracted from the hot-tool surfaces and the weld cycle stopped. After cooling, the specimens were removed from the machine and the ''heated'' surfaces of the specimens examined. Note that the morphologies of the cooled surfaces will differ from those of the molten surfaces — which are the ones that will matter during welding — because of surface tension and shrinkage effects. However, the cooled surface morphologies do

Table 2
Melt phase surface study of 5.8-mm-thick undried and dried PC specimens. A melt penetration of 0.13 mm was used

Hot-tool temperature (°C)	Δl_s (10^{-2} mm)							
	$t_H = 5$ s		$t_H = 10$ s		$t_H = 15$ s		$t_H = 20$ s	
	Undried	Dried	Undried	Dried	Undried	Dried	Undried	Dried
230	5	3	9	9	6	8	9	9
245	9	5	8	3	14	3	10	1
260	9	6	6	15	−3	4	−1	−8
275	−5	4	−4	−5	−5	−37	1	−52
290	−13	−19	−1	−67	3	−50	3	−117
305	−4	−27	4	−51	3	−33	15	−20
320	6	−13	13	−5	14	−5	18	−1
335	9	−36	18	−28	19	−37	15	−37
350	13	−24	18	−22	15	−27	29	−65
365	0	−38	8	−1	19	0	22	0
380	3	6	17	11	22	8	23	−1
395	6	−5	20	15	24	14	27	9
410	3	6	23	18	27	18	29	6
425	1	11	19	8	30	5	29	3
440	14	14	18	10	27	4	34	0

provide an insight into the welding process. The surfaces of the hot-tool were also examined after each test to check for residues and to determine the ease with which the hot-tool surfaces could be cleaned. The changes in lengths of 60 undried and 60 dried specimens, at 15 hot-tool temperatures from 230°C to 440°C in steps of 15°C, with four heating times of 5, 10, 15, and 20 s at each hot-tool temperature, are listed in Table 2. With a melt penetration of 0.13 mm, the

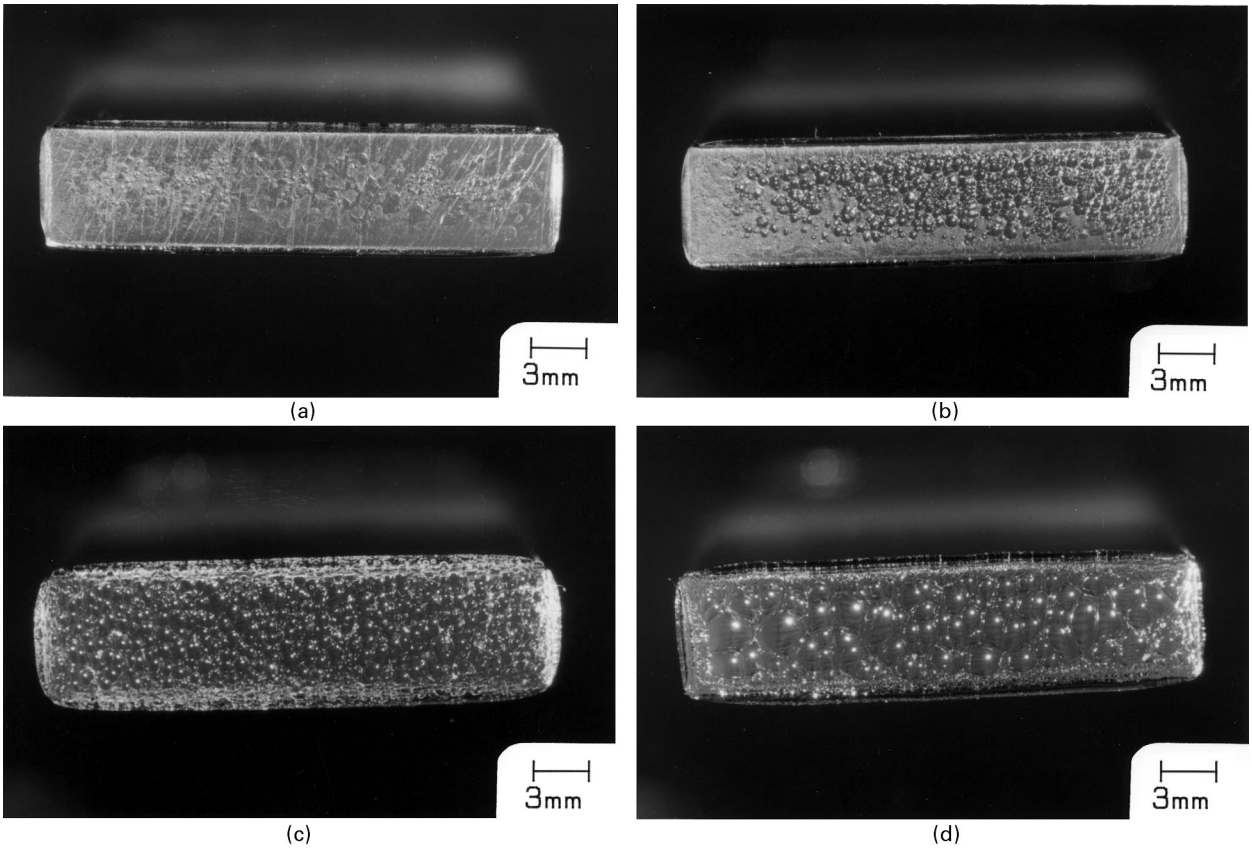

Fig. 3. Solidified molten surface textures of 5.8-mm-thick undried and dried PC specimens. The figures on the left (a, c) and right (b, d) correspond, respectively, to undried and dried specimens. The hot-tool temperatures and the heating times are as follows: (a) and (b) $T_H = 230$°C and $t_H = 5$ s; and (c) and (d) $T_H = 275$°C, $t_H = 15$ s.

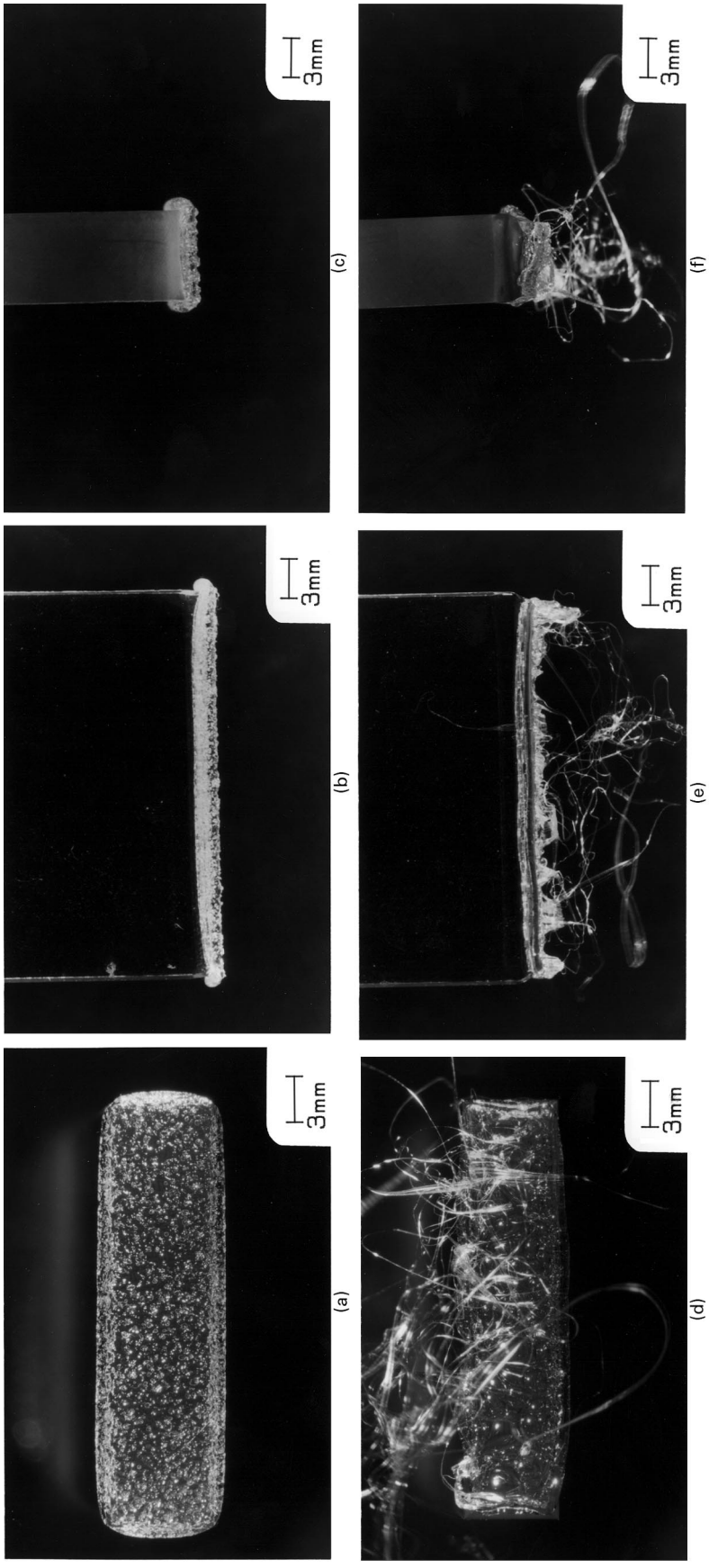

Fig. 4. (a) Solidified molten surface texture of a 5.8-mm-thick undried PC specimen for $T_H = 290°C$ and $t_H = 20$ s; (b) and (c) show the side views. The corresponding views for the dried material are shown, respectively, in (d), (e), and (f). Notice how the material has been drawn out at the edges of the dried material.

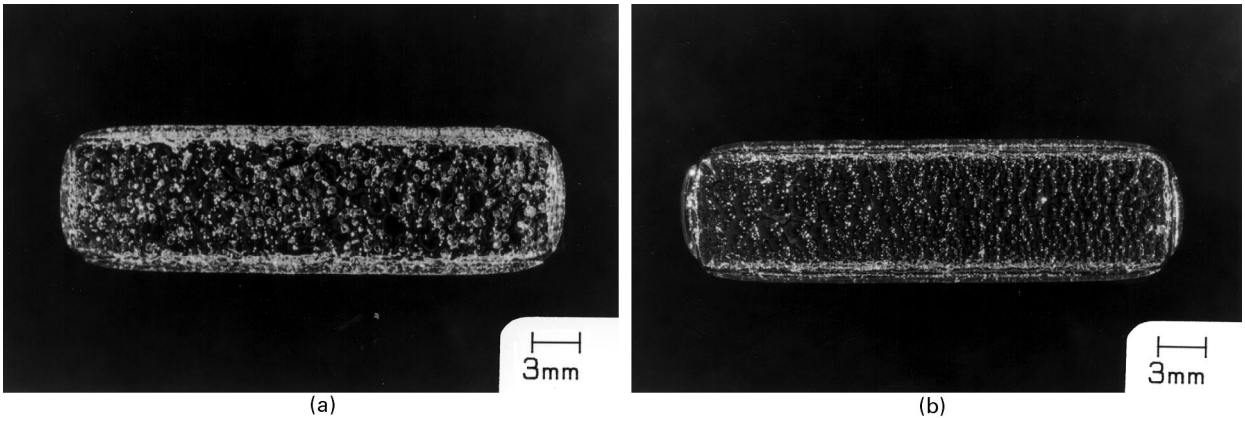

Fig. 5. Solidified molten surface textures of a 5.8-mm-thick undried (a) and dried (b) PC specimen for $T_H = 320°C$ and $t_H = 20$ s.

numbers in columns 2–9 would be expected to not exceed 13. Some of the additional decrease in length beyond 0.13 mm can be attributed to thermal expansion of the heated specimen material in contact with the hot-tool. Other reasons for this decrease are described below.

The solidified molten surfaces exhibited several features. First, large numbers of circular pits, or craters, the numbers and sizes of which changed with the hot-tool temperature and the heating time. Second, at some temperatures ''stringing'' occurred — as the molten surface was pulled away from the hot-tool, very fine fibers were drawn between material sticking to the hot-tool and the molten surface on the specimen. Fig. 3a and b shows the surface features of undried and dried specimens, respectively, for a hot-tool temperature of $T_H = 230°C$ and $t_H = 5$ s. The undried specimen has picked up the surface texture of the hot-tool; the dull surface of the specimen has a small number of shallow, flat depressions. The dried specimen has a larger number of spheroidal craters that intersect in sharp ridges. At this temperature, the number of craters for both the undried and dried specimens increase with heating times. Also, no subsurface bubbles are seen at this hot-tool temperature. As the hot-tool temperature is raised, the number of craters increase: The surface textures at $T_H = 245°C$ are very similar to those at 275°C with some increase in the number of craters. At $T_H = 260°C$ the number of craters increase and more craters can be seen even at $t_H = 5$ s.

The surface textures for $T_H = 275°C$ are different. First, a large number of craters exist even at $t_H = 5$ s; the undried surfaces have more craters. These craters intersect along sharp ridges resulting in local peaks at higher t_H; there are more peaks in the dried material where it was pulled into sharp ''cones''. These sharp cones are precursors to stringing. The morphologies of the molten surfaces for $t_H = 15$ s are shown in Fig. 3c and d — the undried specimen has a large number of small craters while the dried specimen has a smaller number of large craters. Very minor stringing occurs at this temperature, that for the dried material being larger.

Substantial stringing occurs at $T_H = 290°C$. Fig. 4a shows a large number of craters but no evidence of stringing in the undried material for $t_H = 20$ s. The side views in Fig. 4b and c shows the structure of the ''flash'', with very little distortion of the specimens at the edges. The dried material (Fig. 4d) has a smaller number of larger craters accompanied by substantial stringing from the conical peaks. The dried material appears to adhere to the hot-tool surface — as the specimens are pulled away, the molten film is ''drawn'' so that the material near the surface ''necks'', as shown by the side views in Fig. 4e and f. Also, at this temperature, subsurface bubbles can be seen in the undried material; bubbles can also be seen in the flash.

At $T_H = 305°C$, while in contact with the hot-tool surface, the undried material starts to smoke for $t_H > 5$ s. The surface textures are similar to those for $T_H = 290°C$, except that subsurface bubbles can be increasingly seen at higher t_H in the undried material; the dried material does not show any subsurface bubbles. At $T_H = 320°C$, while there is no smoking at $t_H = 5$ s, both the undried and dried materials smoke for $t_H > 5$ s. For $T_H = 320°C$ and $t_H = 5$ s, the surface textures of the undried and dried materials are shown, respectively, in Fig. 5a and b. These surface textures and subsurface bubbles are the same as for 305°C. The textures for $T_H = 335°C$ are also very similar to those for 305°C and 320°C. For $T_H > 320°C$, both the undried and dried materials smoke. For T_H in the range of 305°C–365°C, both the undried and dried materials exhibit stringing, with that in the dried material being more. In this temperature range the stringing is less than in the range of 290°C–305°C.

The surface features at 350°C are similar to those at 335°C — almost no subsurface bubbles at $t_H = 5$ s and increasing bubbles at higher t_H. For a hot-tool temperature of $T_H = 350°C$ and $t_H = 20$ s, the surface features of an undried specimen are shown in Fig. 6. The undried material has a relatively flat surface with flash protruding out parallel to the surface (Fig. 6b and c). The surface of dried material is quite different; it exhibits some stringing. Also, while the size of the craters is about the same as in the undried material, the dried material ''necks'' as in the case of $T_H = 290°C$. At $T_H = 365°C$, there is very little stringing most

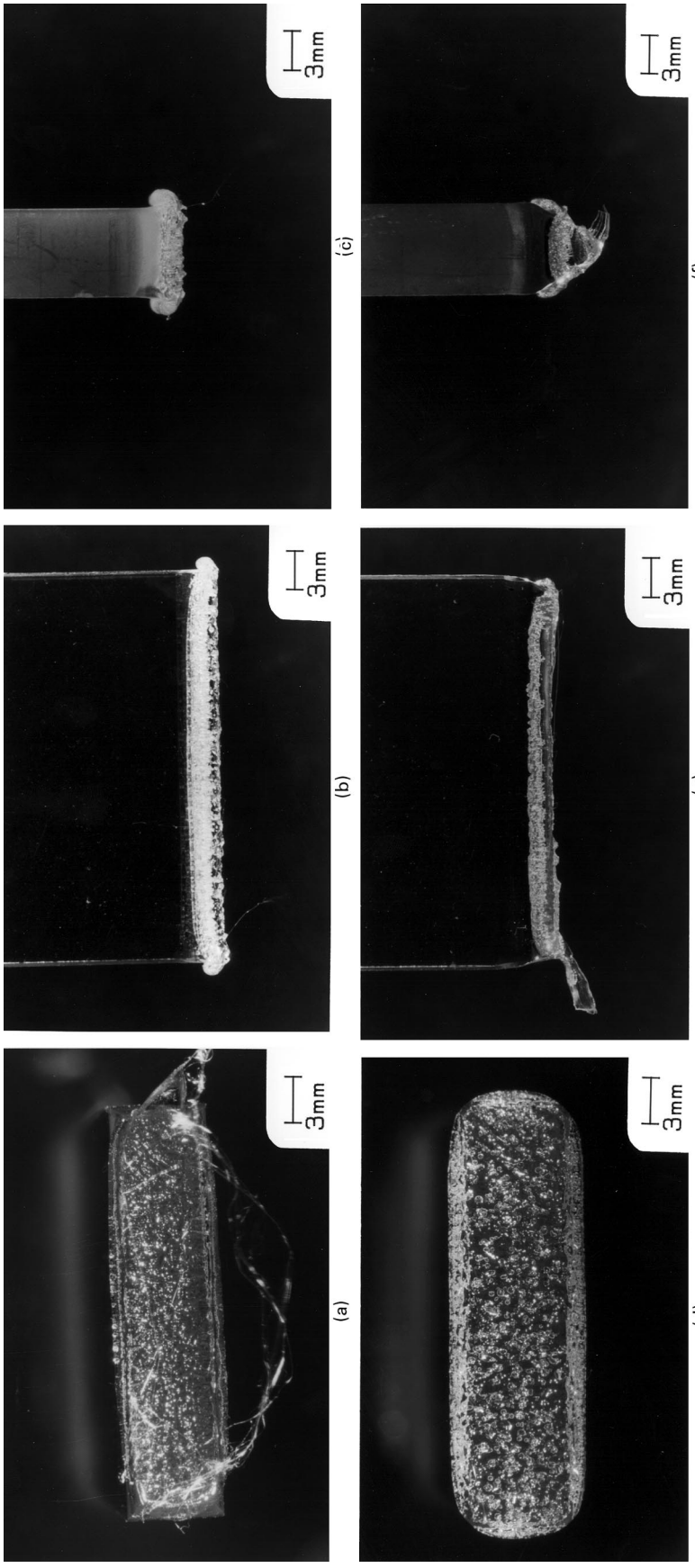

Fig. 6. (a) Solidified molten surface textures of a 5.8-mm-thick undried PC specimen for $T_H = 350°C$ and $t_H = 20$ s; (b) and (c) show the side views. The corresponding views for the dried material are shown, respectively, in (d), (e), and (f). Notice how the material has been drawn out at the edges of the dried material.

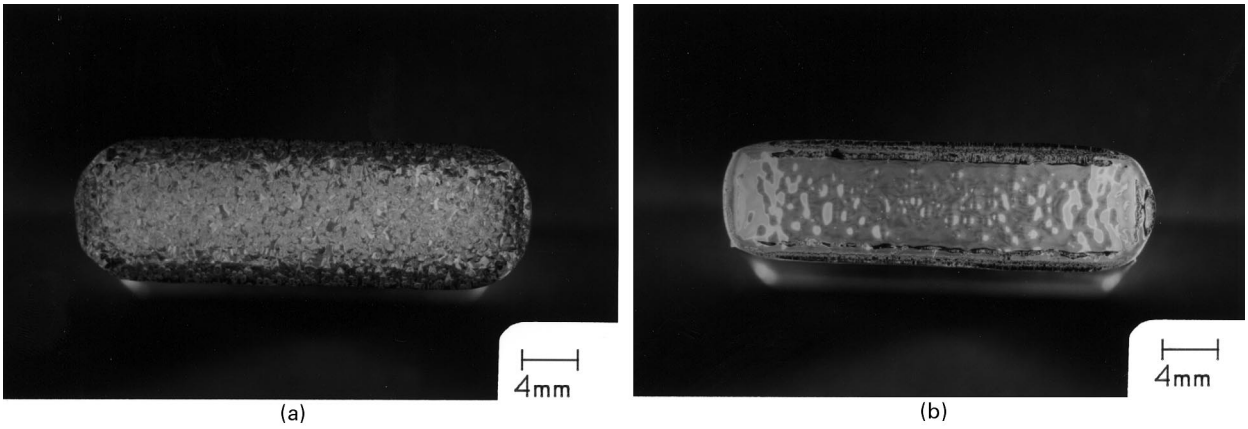

Fig. 7. Solidified molten surface textures of a 5.8-mm-thick undried (a) and dried (b) PC specimen for $T_H = 425°C$ and $t_H = 20$ s.

of which burns off. At $T_H = 380°C$, there is occasional minor stringing that burns off.

For T_H in the range of 395°C–440°C, very little stringing is occasionally seen only for $t_H = 5$ s. In this temperature range, the craters intersect in rounded ridges that do not result in conical peaks from which stringing initiates at lower temperatures. The number of subsurface bubbles in the undried material, which are present even at $t_H = 5$ s, increase rapidly with increases in both t_H and T_H. For $T_H = 425°C$ and $t_H = 20$ s, the relatively ''smooth'' textures of the undried and dried specimen surfaces are shown, respectively, in Fig. 7a and b. Evidence of material degradation at $T_H = 425°C$ and 440°C is provided by an amber colored discoloration of the molten surface. The undried material appears to have a slightly deeper discoloration. Also, the edges (flash) appears to have a deeper discoloration.

As mentioned earlier, with a melt penetration of 0.13 mm, the decreases in the lengths of specimens, Δl_s, listed in Table 2, should not exceed 13 — the additional decrease beyond 0.13 mm resulting from thermal expansion of the heated specimen material in contact with the hot-tool. The data in this table show that, except in a few cases, positive value of Δl_s in the undried material tend to increase with both T_H and t_H — most likely because of more complete melting and thermal expansion effects. However, in the dried material, negative values of Δl_s imply an *increase* in the specimen lengths for T_H in the range of 260°C–395°C. The largest increases occur at temperatures at which the material tends to stick to the hot-tool surface, causing the molten/softened material to neck and draw (Figs. 4e, f and 6e, f), thereby resulting in an apparent increase in the specimen length. This effect accounts for the positive values of Δl_s being lower for the dried material in comparison to those for the undried material. Also, this effect is reflected to some extent in the undried material, and explains the slight deviation from the overall trend.

The results of this molten surface study show clear differences between undried and dried PC. At some temperatures (viscosities), molten PC tends to stick to the hot-tool surface. As the specimen is pulled away from the hot-tool, some portions of the melt separate from the hot-tool surface to form the bottoms of the observed craters — the portions that separate last form the ridges of the craters. Bubbles formed from the moisture in the undried material provide a large number of nucleation sites for the melt to pull away from the tool surface, resulting in a large number of small craters. In contrast, fewer nucleation sites in the dried material results in fewer craters that grow to larger sizes. Also, in the dried material, the fewer ''ridges'' have sharper edges because of more drawing. These sharp ridges tend to form sharp conical peaks from which stringing initiates. This mechanism explains the tendency of the dried material to string far more than the undried material. The tendency of the dried material to stick more also explains the differences of the molten surfaces — relatively flat in the undried material and drawn out edges with a depressed central core in the dried material.

Of importance are deposits on the hot-tool surfaces that could affect the temperature and surface texture seen by the specimen. Also, debris from an unclean surface could be transferred to the molten surface — the resulting contamination could affect weld strength. The hot-tool surfaces were examined and cleaned after each test by using a copper scraper. At $T_H = 230°C$, the surfaces could be cleaned easily for $t_H = 5$, 10, and 15 s; cleaning of the undried material was somewhat easier. Cleaning became more difficult at $t_H = 20$ s. For T_H from 245°C to 275°C, material smeared onto the hot-tool surfaces and was very difficult to clean. The amount of material left on the hot-tool surfaces decreased for T_H from 290°C to 305°C. For T_H from 320°C to 350°C the deposits had a very rough texture. For $T_H > 365°C$, the deposits had a mixture of smeared and rough texture.

In summary, in comparison to undried specimens, the dried specimens had larger surface craters, fewer bubbles in the flash, and exhibited more stringing that started at $T_H = 275°C$. As the hot-tool temperature was increased, the material deposited on the surface tended to smear than be scraped off during cleaning: this smearing started at about $T_H = 260°C$. Smoking at the hot-tool surface started at about 305°C and 320°C for the undried and dried materials,

Table 3
Strength and ductility data for hot-tool welds of 3-mm-thick undried and dried PC specimens, at a strain rate of $\dot{\varepsilon} = 0.01\ s^{-1}$, as functions of the hot-tool temperature and the heating time. The melt and weld penetrations were maintained at 0.13 and 0.25 mm, respectively, and the seal time was kept constant at 10 s

Hot-tool temperature (°C)	Heating time (s)	Weld strength[a] (MPa)		Failure strain[b] (%)		Δl (mm)		Differential penetration $\Delta\eta$ ($\Delta\eta_T$) (10^{-2} mm)	
		Undried	Dried	Undried	Dried	Undried	Dried	Undried	Dried
200	10	[c]	[c]	[c]	[c]	[c]	[c]	[c]	[c]
215	10	25.6	19.3	1.23	0.89	0.71	0.69	5 (13)	8 (16)
230	10	28.9	37.2	1.34	1.84	0.81	0.79	−5 (3)	−3 (5)
245	10	41.0	53.0	2.25	3.06	0.93	0.93	−17 (−7)	−17 (−7)
260	10	41.6	38.4	2.36	2.08	0.89	0.89	−13 (−3)	−13 (−3)
275	10	49.3	52.1	3.20	2.96	1.02	0.99	−25 (−13)	−23 (−11)
290	10	49.4	64.5	3.15	4.62[d]	1.04	0.98	−28 (−16)	−22 (−10)
305	10	43.3	60.8	2.61	4.40	0.89	0.98	−13 (−1)	−22 (−10)
320	10	27.4	48.7	1.40	3.33	1.02	1.09	−25 (−11)	−33 (−19)
335	10	—	63.2	—	4.68[d]	—	1.16	—	−39 (−25)
200	15	18.9	[c]	0.79	[c]	0.64	[c]	13 (23)	[c]
215	15	20.8	22.1	0.95	1.02	0.79	0.74	−3 (7)	3 (13)
230	15	29.9	46.1	1.47	2.37	0.90	0.89	−14 (−2)	−13 (−1)
245	15	37.4	55.8	1.95	3.36	0.95	0.95	−19 (−7)	−19 (−7)
260	15	40.5	36.2	2.39	2.17	0.93	0.90	−17 (−3)	−14 (0)
275	15	47.4	50.3	3.40	3.38	1.05	1.02	−29 (−15)	−25 (−11)
290	15	40.1	59.2	2.43	4.10	1.07	0.98	−30 (−16)	−22 (−8)
305	15	36.1	61.8	2.10	4.45[d]	0.94	1.02	−18 (−2)	−25 (−9)
320	15	18.6	57.4	0.90	5.03	0.94	1.07	−18 (−2)	−30 (−14)
335	15	—	62.5	—	4.52[d]	—	1.17	—	−41 (−23)
200	20	24.7	13.8	1.12	0.62	0.67	0.71	9 (21)	5 (17)
215	20	26.8	28.5	1.24	1.37	0.84	0.83	−8 (4)	−6 (6)
230	20	30.4	45.1	1.48	2.43	0.90	0.95	−14 (0)	−19 (−5)
245	20	33.7	44.8	1.80	2.40	0.95	0.99	−19 (−5)	−29 (−15)
260	20	43.8	34.1	2.75	1.71	0.98	0.99	−22 (−6)	−29 (−13)
275	20	48.6	59.9	3.20	4.34	1.04	1.02	−28 (−12)	−25 (−9)
290	20	23.2	62.4	1.20	4.49[d]	1.05	1.02	−29 (−11)	−25 (−7)
305	20	31.1	61.2	1.93	4.96	0.99	1.00	−23 (−5)	−24 (−6)
320	20	12.8	63.2	0.63	5.58[d]	0.97	1.10	−20 (−2)	−34 (−16)
335	20	—	62.8	—	4.80[d]	—	1.16	—	−39 (−19)

[a] $\sigma_0 = 63.6$ MPa.
[b] $\varepsilon_0 = 6.65\%$.
[c] Very low strength; specimen broke during routing.
[d] Specimen yielded at the weld before breaking at the weld.

respectively. Tiny bits of debris of burned PC appeared sporadically on specimen surfaces for T_H from 365°C to 440°C. While in contact with the hot-tool surface, a molten film of material was visible at the hot-tool/specimen interface. This film thickened with an increase in the heating time, and the thickening was achieved faster at higher hot-tool temperatures.

5. Weld strength

In this paper, the total time $t_H = t_0 + t_M \approx t_M$ for which the specimen is in contact with the hot-tool will be referred to as the heating time; melt penetration will refer to the distance δ_0 (Fig. 2); weld penetration will refer to the distance δ_H; and the time t_w will be referred to as the seal time. For most of the data in this paper, the process parameters were varied as follows: Hot-tool temperatures from $T_H = 200$°C to 410°C; heating times of $t_H = 10$, 15, and 20 s; a melt penetration of $\delta_0 = 0.13$ mm; two weld penetrations of $\delta_H = 0.25$ and 0.66 mm; and a seal time of $t_w = 10$ s. In addition, a limited number of tests were done at $t_H = 5$ and 30 s; $\delta_0 = 0.38$ mm; and $t_w = 5$, 15, and 20 s. Of the three thicknesses of 3-, 5.8-, and 12-mm, the largest amount of data was obtained on 5.8-mm-thick specimens.

5.1. 3-mm-thick specimens

Strength and ductility data for 3-mm-thick undried and dried PC specimens, at a nominal strain rate of $0.01\ s^{-1}$, as functions of the hot-tool temperature and the heating time, are listed in Table 3. The PC specimens had a yield strength

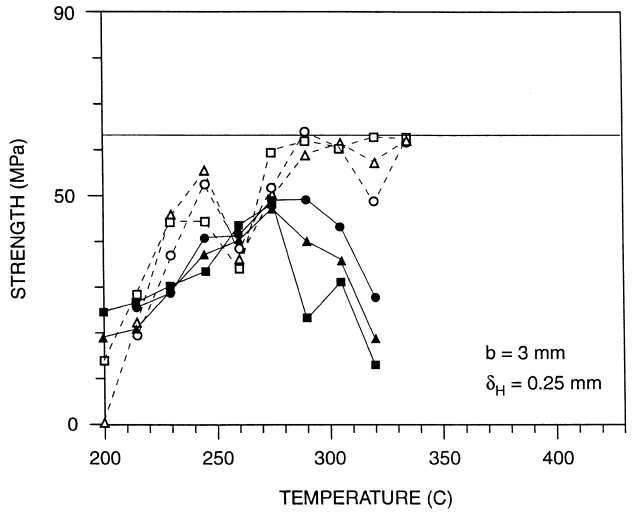

Fig. 8. Weld strength of 3-mm-thick undried (solid symbols) and dried (open symbols) PC as a function of the hot-tool temperature, with the heating time as parameter. Circles, triangles and squares correspond, respectively, to heating times of 10, 15, and 20 s. The melt and weld penetrations were maintained at 0.13 and 0.25 mm, respectively.

of $\sigma_0 = 63.6$ MPa and a yield strain of $\epsilon_0 = 6.65\%$. The melt and weld penetrations were maintained at 0.13 and 0.25 mm, respectively, and the seal time was kept constant at 10 s. The first column in this table shows that the hot-tool temperature was varied between 200°C and 335°C. The second column shows the three heating times used (10, 15, and 20 s). For the undried material, columns 3, 5, 7, and 9 list, respectively, the weld strength, the failure strain, the change in length Δl after welding, and the differential penetrations $\Delta\eta$ and $\Delta\eta_T$. Columns 4, 6, 8, and 10 list the corresponding data for the dried material.

Fig. 8 shows the weld strength (data from Table 3) of the undried (solid symbols) and dried (open symbols) specimens as a function the hot-tool temperature for three heating times of 10, 15, and 20 s (indicated respectively, by circles, triangles, and squares). The thin horizontal line represents the strength of the resin (63.6 MPa). Strength and ductility data for a higher weld penetration of 0.66 mm, all other parameters being the same as in Table 3, are listed in Table 4. The corresponding variation of the weld strength with the hot-tool temperature is shown in Fig. 9. Note that the data in Tables 3 and 4, which were obtained from one test per test condition studied, do not provide information on the variability in the weld strength at each test condition.

Thus, Figs. 8 and 9 compare the effect of the weld penetration (0.25 and 0.66 mm, respectively), all other weld parameters being the same. First, for the same set of process conditions, these two figures show that higher weld strengths are obtained in the dried material. For example, for a weld penetration of 0.25 mm, while the highest relative weld strength obtained for the undried material was 78% of the material strength ($T_H = 275$°C–290°C, $t_H = 10$ s), very high strengths — even exceeding 100% — were obtained for the dried material over a much wider process window ($T_H = 275$°C–335°C, $t_H = 10$, 15, 20 s). Also, a comparison of the strains to failure in columns 5 and 6 in Table 3 shows that the welds in the dried material exhibit more ductility (larger strains to failure). Second, higher weld strengths are obtained at the larger weld penetration of 0.66 mm — relative strengths greater than 100% were obtained both for the undried ($T_H = 230$°C–290°C) and dried materials ($T_H = 260$°C–305°C). In this case, the welds in both the undried and dried specimens exhibit high ductility. Thus, 3-mm-thick PC parts do not have to be dried before welding if the right hot-tool temperatures are used.

The data in Table 4 show weld strengths up to 70 MPa for a material with a nominal yield strength of $\sigma_0 = 63.6$ MPa. While some of the higher weld strength could be attributed to variations in σ_0, most of the high apparent strength results from an increase in the weld cross section caused by a thickening of the weld zone contributed by the flash, or weld bead. This increase in strength was demonstrated for a different material [26] by comparing strengths of welded specimens with the flash retained with those with the flash machined off. For the same weld process conditions, thinner specimens thicken more, and may therefore attain higher apparent strengths.

Fig. 10 shows the fracture surfaces of 3-mm-thick undried and dried specimens that were welded at the higher weld penetration of 0.66 mm and a heating time of $t_H = 10$ s. The figures on the left (a, c) and right (b, d) correspond, respectively, to undried and dried specimens. Fig. 10a and b, which show similar morphologies, correspond to a hot-tool temperature of $T_H = 260$°C, at which (row 5 in Table 4) the undried and dried specimens have comparable high strengths (63.3 and 69.5 MPa) and very high strains to failure (6.75% and 5.30%). The different morphologies in Fig. 10c and d correspond to a hot-tool temperature of $T_H = 305$°C, at which (row 8 in Table 4) the undried and dried specimens have very different strengths (31.5 and 69.8 MPa) and failure strains (1.52% and 5.72%). The fracture surface of the undried material, which exhibits the lower weld strength, shows evidence of voids and has white parallel streaks. The mechanism of failure in the three high-strength welds appears to be the same — uniaxial extension in which small voids grow in triaxial stress fields, followed by fast fracture.

The molten surfaces of 5.8-mm-thick, undried and dried specimens begin to exhibit some stringing at a hot-tool temperature of $T_H = 275$°C. Substantial stringing occurs at $T_H = 295$°C in the dried material (Fig. 4d–f). Both the undried and dried materials exhibit stringing for T_H in the range of 305°C–365°C, with more stringing occurring in the dried material. However, the stringing in this range is less than in the range of 295°C–305°C. Since stringing and void formation mainly depend on the temperature, similar behavior can be expected in 3-mm-thick specimens. A perusal of the data in Table 3 (rows 6–10, 16–20, and 26–30) and Table 4 (rows 6–8, 14–16, and 22–24) shows that the dried material — which strings more — exhibits very high

Table 4
Strength and ductility data for hot-tool welds of 3-mm-thick undried and dried PC specimens, at a strain rate of $\dot{\varepsilon} = 0.01\ s^{-1}$, as functions of the hot-tool temperature and the heating time. The melt and weld penetrations were maintained at 0.13 and 0.66 mm, respectively, and the seal time was kept constant at 10 s

Hot-tool temperature (°C)	Heating time (s)	Weld strength[a] (MPa)		Failure strain[b] (%)		Δl (mm)		Differential penetration $\Delta\eta$ ($\Delta\eta_T$) (10^{-2} mm)	
		Undried	Dried	Undried	Dried	Undried	Dried	Undried	Dried
200	10	[c]	[c]	[c]	[c]	[c]	[c]	[c]	[c]
215	10	18.9	8.7	0.83	0.39	0.99	0.66	58 (64)	91 (99)
230	10	24.4	19.7	1.20	0.94	1.33	1.19	24 (32)	38 (46)
245	10	40.8	42.6	2.17	2.20	1.50	1.41	8 (18)	17 (27)
260	10	63.3	69.5	6.75[d]	5.30	1.54	1.57	4 (14)	0 (10)
275	10	62.6	69.8	6.08[e]	5.32[d]	1.61	1.57	−4 (8)	3 (15)
290	10	63.5	70.0	6.05[e]	5.43[d]	1.71	1.68	−14 (−2)	−10 (2)
305	10	31.5[f]	69.8	1.52	5.72[d]	1.73	1.66	−15 (−3)	−9 (3)
200	15	[c]	[c]	[c]	[c]	[c]	[c]	[c]	[c]
215	15	18.2	23.6	0.81	1.15	1.21	1.07	37 (47)	51 (61)
230	15	36.8	43.1	1.81	2.28	1.46	1.35	11 (23)	23 (35)
245	15	63.5	68.4	5.91[e]	4.91	1.56	1.57	1 (13)	0 (12)
260	15	63.2	69.0	6.16[e]	5.20	1.63	1.64	−5 (9)	−6 (8)
275	15	64.1	69.0	6.23[e]	5.07[d]	1.60	1.60	−3 (11)	−3 (11)
290	15	63.3	69.0	6.32[d]	5.33[d]	1.70	1.66	−13 (1)	−9 (5)
305	15	23.2	69.0	1.09	5.78[d]	1.75	1.73	−18 (−2)	−15 (1)
200	20	[c]	[c]	[c]	[c]	[c]	[c]	[c]	[c]
215	20	30.0	24.3	1.41	1.18	1.42	1.21	15 (27)	37 (49)
230	20	66.9	55.6	4.55	3.11	1.55	1.45	3 (17)	13 (27)
245	20	67.7	69.3	4.99	5.49	1.64	1.65	−6 (8)	−8 (6)
260	20	63.5	55.2	6.55[d]	3.04[g]	1.65	1.63	−8 (10)	−5 (11)
275	20	63.4	68.9	5.63[e]	4.96[d]	1.69	1.68	−11 (5)	−10 (6)
290	20	39.8	69.6	2.27	5.90[d]	1.68	1.66	−10 (8)	−9 (9)
305	20	16.3	68.9	0.76	5.38[d]	1.73	1.71	−15 (3)	−14 (4)

[a] $\sigma_0 = 63.6$ MPa.
[b] $\varepsilon_0 = 6.65\%$.
[c] Very low strength; specimen broke during routing.
[d] Specimen yielded at the weld before breaking at the weld.
[e] Specimen yielded outside the weld.
[f] Weld surface had white parallel streaks.
[g] Specimen had debris on weld surface.

weld strengths for T_H in the range of 295°C–335°C. Thus, stringing does not result in reduced weld strength. In the undried material, reduced weld strengths at higher weld temperatures correlates with increasing number of smaller bubbles.

Earlier, it was argued that, *if* thermal expansion effects are neglected, then the differential penetration $\Delta\eta \geq 0$, and that stops do and do not contact when $\Delta\eta = 0$ and $\Delta\eta > 0$, respectively. However, when thermal expansion at the heated ends of the specimens is accounted for, a better measure for whether or not stops come into contact is $\Delta\eta_T \geq 0$. The last two columns in Table 3 (data for the smaller weld penetration of 0.25 mm) show mostly negative values of $\Delta\eta$, except at the lowest temperatures, for both the undried and dried specimens. Although the corresponding values of $\Delta\eta_T$ are larger, as expected, they are still mostly negative. For the larger weld penetration of 0.66 mm, the last two columns in Table 4 show that while $\Delta\eta$ is still negative at higher temperatures, $\Delta\eta_T$ is negative only for three data points for the undried material.

One explanation for this discrepancy would be errors in the measurements of δ_0 and the weld penetration δ_H. Instead of the two stops shown in the schematic in Fig. 2, contact is actually determined by four stops on each side. The difficulty in establishing even contact among the four stops on each side could result in errors in δ_0 and δ_H. A combined small increase of $\delta = \delta_0 + \delta_H = 0.1$ mm would make almost all values of $\Delta\eta_T$ greater than or equal to zero. This argument is supported by the data in Tables 3 and 4 that show that $\Delta\eta_T$ is positive for the larger weld penetration of 0.66 mm — any systematic error in the measurements would be a smaller fraction of larger settings.

The data in the last two columns of Tables 3 and 4 do show the following trends that are consistent with expectations based on the underlying physics: First, at any fixed heating time t_H, $\Delta\eta_T$ decreases with increases in the

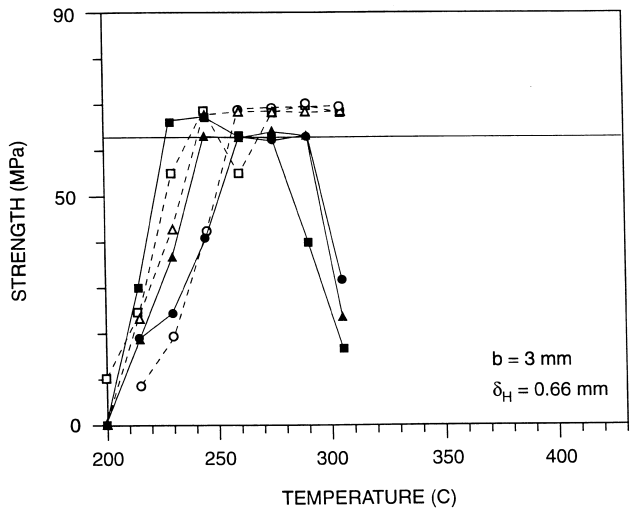

Fig. 9. Weld strength of 3-mm-thick undried (solid symbols) and dried (open symbols) PC as a function of the hot-tool temperature, with the heating time as parameter. Circles, triangles and squares correspond, respectively, to heating times of 10, 15 and 20 s. The melt and weld penetrations were maintained at 0.13 and 0.66 mm, respectively.

hot-tool temperature T_H. This is to be expected because higher temperatures result in thicker molten layers, thereby allowing for the hot-tool stops to come closer before the melt freezes off. Second, for a fixed hot-tool temperature, $\Delta\eta_T$ again decreases with increases in the melt time; this is explained by increased heating times resulting in thicker molten films.

5.2. 5.8-mm-thick specimens

Strength and ductility data for 5.8-mm-thick undried and dried PC specimens as functions of the hot-tool temperature and the heating time are listed in Tables 5 and 6 for weld penetrations of 0.25 and 0.66 mm, respectively. The PC specimens had a yield strength of 66.5 MPa, higher than that of the 3-mm-thick specimens, and a yield strain of 7%. The melt penetration was maintained at 0.13 mm and the seal time was kept constant at 10 s. In contrast to 3-mm-thick specimens, the hot-tool temperature was varied between 215°C and 410°C.

Just as in the case of 3-mm-thick specimens, note that the

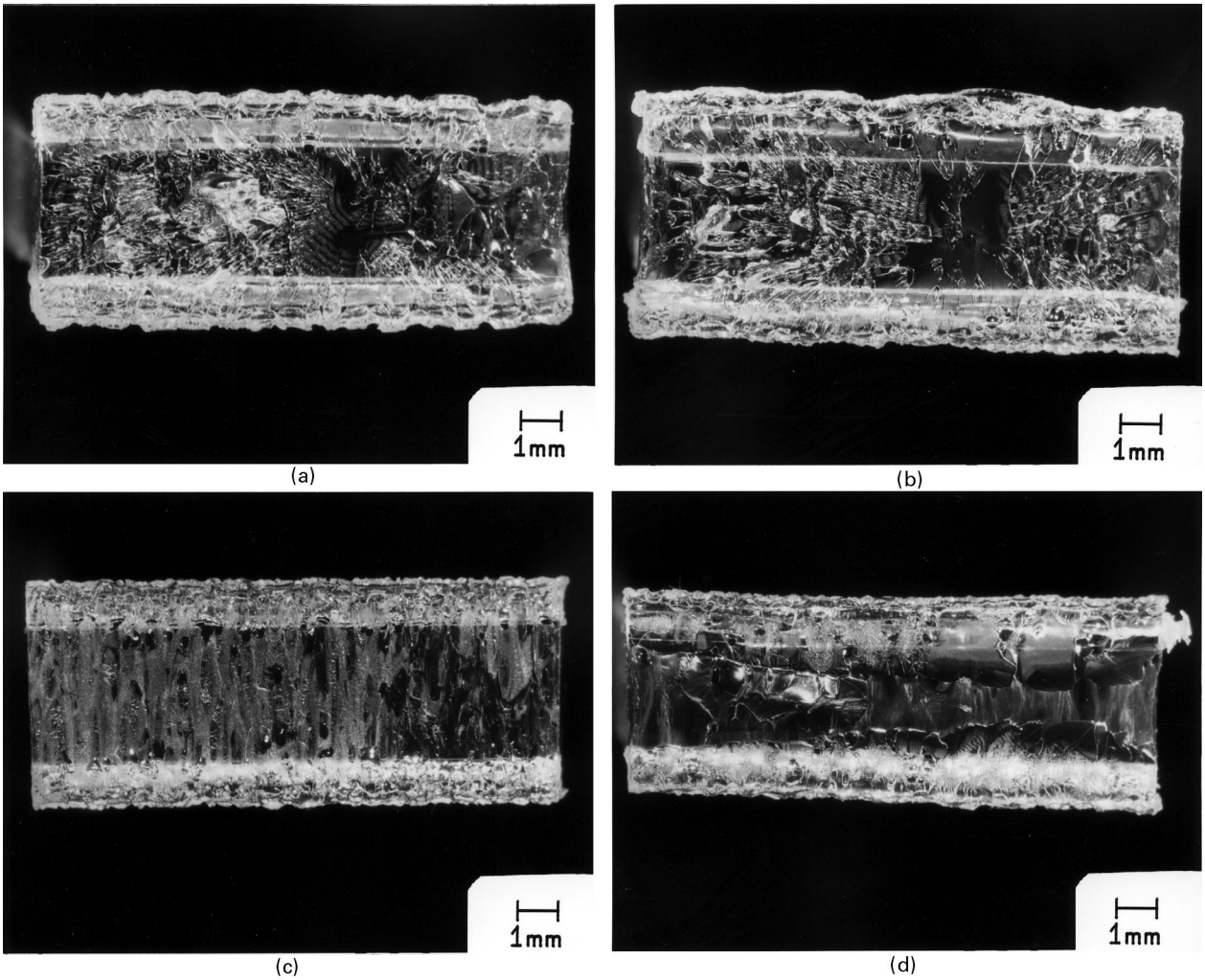

Fig. 10. Fracture surfaces of 3-mm-thick undried and dried PC specimens. The figures on the left (a, c) and right (b, d) correspond, respectively, to undried and dried specimens. The heating time was $t_H = 10$ s and the hot-tool temperatures were $T_H = 260$°C for (a) and (b) and $T_H = 305$°C for (c) and (d).

Table 5
Strength and ductility data for hot-tool welds of 5.8-mm-thick undried and dried PC specimens, at a strain rate of $\dot{\varepsilon} = 0.01\ s^{-1}$, as functions of the hot-tool temperature and the heating time. The melt and weld penetrations were maintained at 0.13 and 0.25 mm, respectively, and the seal time was kept constant at 10 s

Hot-tool temperature (°C)	Heat time (s)	Weld strength[a] (MPa)		Failure strain[b] (%)		Δl (mm)		Differential penetration $\Delta\eta$ ($\Delta\eta_T$) (10^{-2} mm)	
		Undried	Dried	Undried	Dried	Undried	Dried	Undried	Dried
215	10	21.9	17.2	0.98	0.81	0.38	0.36	38 (46)	40 (48)
230	10	42.4	38.8	2.08	1.86	0.70	0.64	6 (16)	13 (23)
245	10	60.6	41.7	3.98	1.98	0.81	0.80	−5 (5)	−4 (6)
260	10	46.7	57.3	2.51	3.20	0.84	0.93	−8 (2)	−17 (−7)
275	10	43.4	55.8	2.20	3.03	0.95	1.00	−19 (−7)	−24 (−12)
290	10	33.6	52.0	1.56	2.69	0.93	0.97	−17 (−5)	−20 (−8)
305	10	22.9	59.1	1.00	3.25	0.94	1.04	−18 (−6)	−28 (−16)
320	10	16.2	57.0	0.71	3.10	0.95	0.99	−19 (−5)	−23 (−9)
335	10	17.2	59.6	0.76	3.42	0.99	1.03	−23 (−9)	−27 (−13)
350	10	28.4	31.3	1.34	1.49	1.00	0.98	−24 (−10)	−22 (−12)
365	10	29.1	46.4	1.39	2.34	1.00	0.99	−24 (−8)	−23 (−13)
380	10	26.9	61.9	1.25	3.64	1.04	1.14	−28 (−12)	−38 (−22)
395	10	43.1	43.8	2.73	2.22	1.03	1.09	−27 (−11)	−33 (−17)
410	10	42.8	58.4	2.95	3.32	1.10	1.01	−34 (−16)	−25 (−7)
215	15	22.9	21.1	1.03	0.95	0.65	0.64	11 (21)	13 (23)
230	15	58.7	40.3	3.76	1.93	0.79	0.81	−3 (9)	−5 (7)
245	15	56.4	30.9	3.47	1.59	0.85	0.90	−9 (3)	−14 (−2)
260	15	41.9	54.8	2.20	2.88	0.95	0.90	−19 (−5)	−14 (0)
275	15	39.5	43.0	2.03	2.05	0.95	0.98	−19 (−5)	−22 (−28)
290	15	27.3	44.6	1.25	2.37	0.98	1.05	−22 (−8)	−27 (−13)
305	15	21.7	43.1	1.00	2.12	1.04	0.99	−28 (−12)	−23 (−7)
320	15	21.3	50.0	1.00	2.59	1.05	1.01	−27 (−11)	−25 (−9)
335	15	27.0	48.6	1.27	2.47	1.08	1.07	−32 (−14)	−30 (−12)
350	15	22.8	55.7	1.10	3.12	1.03	1.05	−27 (−9)	−27 (−9)
365	15	23.7	46.5	1.12	2.42	0.99	1.05	−23 (−3)	−27 (−7)
380	15	27.6	65.5	1.32	4.27	1.12	1.21	−36 (−16)	−44 (−24)
395	15	33.3	60.0	1.66	3.76	1.08	1.05	−32 (−12)	−27 (−7)
410	15	26.0	63.1	1.32	4.22	1.08	1.13	−32 (−10)	−37 (−15)
215	20	38.3	[c]	1.83	[c]	0.79	[c]	−3 (9)	[c]
230	20	52.4	48.2	2.95	2.39	0.90	0.88	−14 (0)	−11 (3)
245	20	46.6	56.1	2.37	3.12	0.95	0.88	−19 (−5)	−11 (3)
260	20	39.2	44.2	1.95	2.20	0.89	0.99	−13 (3)	−23 (−7)
275	20	22.4	43.8	1.07	2.10	0.97	1.01	−20 (−4)	−25 (−9)
290	20	14.1	47.4	0.61	2.51	0.94	1.03	−18 (0)	−27 (−9)
305	20	16.1	48.1	0.76	2.44	0.98	1.14	−22 (−4)	−38 (−20)
320	20	15.0	62.6	0.68	3.71	1.01	1.01	−25 (−7)	−25 (−7)
335	20	22.8	60.5	1.10	3.64	1.08	1.05	−32 (−12)	−27 (−7)
350	20	25.5	59.0	1.20	3.52	1.12	1.09	−36 (−14)	−33 (−11)
365	20	17.0	50.0	0.85	2.71	1.04	1.08	−28 (−6)	−32 (−10)
380	20	19.9	65.3	0.98	4.59	1.13	1.13	−37 (−15)	−37 (−15)
395	20	27.0	59.9	1.34	3.44	1.14	1.00	−38 (−14)	−24 (0)
410	20	17.2	61.2	0.85	4.30	1.08	1.08	−32 (−8)	−32 (−8)

[a] $\sigma_0 = 66.5$ MPa.
[b] $\varepsilon_0 = 7\%$.
[c] Specimen did not weld.

data for 5.8-mm-thick specimens in Table 5, which were obtained from one test per test condition studied, do not provide information on the variability in the weld strength at each test condition. However, data for a limited number of repeat tests on dried specimens in Table 6 show that weld strength can vary widely for the same weld process conditions: weld strengths of 47.1 and 72.0 MPa at $T_H = 320$°C and $t_H = 10$ s; 72.6 and 72.0 MPa at $T_H = 350$°C and $t_H = 10$ s; 39.2, 40.0, and 65.0 MPa at $T_H = 350$°C and $t_H = 15$ s; 33.0, 53.0, and 68.7 MPa at $T_H = 320$°C and $t_H = 20$ s; and 49.2 and 68.8 MPa at $T_H = 350$°C and $t_H = 20$ s. In view of this variability, the number of significant figures in the reported strength is open to question. As such, the data

Table 6
Strength and ductility data for hot-tool welds of 5.8-mm-thick undried and dried PC specimens, at a strain rate of $\dot{\varepsilon} = 0.01\ s^{-1}$, as functions of the hot-tool temperature and the heating time. The melt and weld penetrations were maintained at 0.13 and 0.66 mm, respectively, and the seal time was kept constant at 10 s

Hot-tool temperature (°C)	Heating time (s)	Weld strength[a] (MPa)		Failure strain[b] (%)		Δl (mm)		Differential penetration $\Delta\eta$ ($\Delta\eta_T$) (10^{-2} mm)	
		Undried	Dried	Undried	Dried	Undried	Dried	Undried	Dried
215	10	18.0	—	0.85[c]	—	0.48	—	109 (117)	—
230	10	32.6	29.5	1.56[c]	1.39	0.72	0.75	85 (95)	83 (93)
245	10	42.2	40.1	2.15	1.85	0.99	1.45	58 (68)	13 (23)
260	10	32.1	43.0	1.49	2.03	1.31	1.74	27 (37)	−17 (−7)
275	10	66.3	72.4	6.45[d]	5.69[d]	1.46	1.55	11 (23)	3 (15)
290	10	66.1	74.1	6.03[d]	5.36	1.63	1.59	−5 (7)	−1 (11)
305	10	65.5	72.8	6.15[d]	5.93[d]	1.57	1.71	1 (13)	−14 (−2)
320	10	28.8	47.1	1.20	2.29[e]	1.62	1.71	−4 (10)	−14 (0)
320	10	—	72.0	—	5.66[d]	—	1.69	—	−11 (3)
335	10	22.1	72.6	0.93	5.52[d]	1.71	1.70	−14 (0)	−13 (1)
350	10	17.9	72.6	0.82	5.25	1.64	1.77	−7 (7)	−19 (−5)
350	10	—	72.0	—	5.40[d]	—	1.77	—	−19 (−5)
365	10	—	71.4	—	5.10	—	1.85	—	−28 (−12)
380	10	—	71.3	—	5.32[d]	—	1.85	—	−28 (−12)
395	10	—	70.0	—	5.22[d]	—	1.82	—	−24 (−8)
410	10	—	69.6	—	5.05[d]	—	1.91	—	−33 (−15)
425	10		71.3		5.13[d]		1.83		−25 (−7)
215	15	27.7	—	1.34[c]	—	0.66	—	91 (101)	—
230	15	36.2	32.1	1.71[c]	1.42	1.05	1.68	52 (64)	−10 (2)
245	15	66.0	57.6	5.91	3.01	1.36	1.82	22 (34)	−24 (−12)
260	15	43.3	72.9	2.20	6.50[d]	1.50	1.87	8 (22)	−29 (−15)
275	15	66.6	72.6	6.03[d]	4.83	1.61	1.54	−4 (10)	4 (18)
290	15	65.0	72.8	5.47	5.46	1.69	1.69	−11 (3)	−11 (3)
305	15	52.1	72.0	3.07	5.37[d]	1.67	1.75	−10 (6)	−18 (−2)
320	15	26.1	44.2	1.18	2.12[e]	1.69	1.74	−11 (5)	−17 (−1)
320	15	—	67.7	—	4.47	—	1.77	—	−19 (−3)
335	15	14.5	61.7	0.60	3.34	1.72	1.84	−15 (3)	−27 (−9)
350	15	13.2	39.2	0.55	1.81[e]	1.72	1.80	−15 (3)	−23 (−5)
350	15	—	40.0	—	1.90[c]	—	1.75	—	−18 (0)
350	15	—	65.0	—	4.30	—	1.80	—	−23 (−5)
365	15	—	70.9	—	5.42[d]	—	1.88	—	−30 (−10)
380	15	—	67.4	—	4.61[d]	—	1.85	—	−28 (−8)
395	15	—	59.9	—	3.17[e]	—	1.84	—	−27 (−7)
410[f]	15	—	68.8	—	5.27[d]	—	1.85	—	−28 (−6)
425[f]	15	—	70.2	—	5.27[d]	—	1.87	—	−29 (−7)
215	20	28.1	—	1.32[c]	—	0.99	—	58 (70)	—
230	20	44.0	45.1	2.20	2.12	1.33	1.98	24 (38)	−41 (−27)
245	20	66.2	70.2	6.05	5.22	1.55	1.69	3 (17)	−11 (3)
260	20	28.2	71.5	1.29	6.61[d]	1.66	2.10	−9 (7)	−52 (−36)
275	20	65.8	73.1	5.83[d]	5.25	1.73	1.69	−15 (1)	−11 (5)
290	20	42.5	71.6	2.10	4.89	1.77	1.70	−19 (−1)	−13 (5)
305	20	35.5	62.9	1.67	3.59[e]	1.70	1.77	−13 (5)	−19 (−1)
320	20	13.0	33.0	0.56	1.56[e]	1.71	1.78	−13 (5)	−20 (−2)
320	20	—	53.0	—	2.83[c]	—	1.79	—	−22 (−4)
320	20	—	68.7	—	5.03[d]	—	1.79	—	−22 (−4)
335	20	13.0	66.9	0.56	4.20	1.70	1.83	−12 (8)	−25 (−5)
350	20	13.7	49.2	0.58	2.59	1.75	1.84	−18 (4)	−27 (−5)
350	20	—	68.8	—	4.79	—	1.85	—	−28 (−6)
365	20	—	69.7	—	4.91[d]	—	1.85	—	−28 (−6)
380	20	—	68.0	—	4.69	—	1.87	—	−29 (−7)
395[f]	20	—	66.6	—	4.35[d]	—	1.88	—	−30 (−6)
410[f]	20	—	69.2	—	4.81[d]	—	1.93	—	−36 (−12)
425[f]	20	—	69.2	—	5.08[d]	—	1.77	—	−19 (7)

[a] $\sigma_0 = 66.5$ MPa.
[b] $\varepsilon_0 = 7\%$.
[c] Specimen had debris on weld surface.
[d] Specimen yielded at the weld before breaking at the weld.
[e] Weld surface had white parallel streaks.
[f] Specimen sagged immediately after the joining phase.

Table 7
Strength and ductility data for hot-tool welds of 5.8-mm-thick undried PC specimens, at a strain rate of $\dot{\varepsilon} = 0.01\ s^{-1}$, as functions of the hot-tool temperature and the heating time, for two weld penetrations of 0.25 and 0.66 mm. The melt penetration was maintained at 0.13 mm and the seal time was kept constant at 10 s. A set of five specimens were tested at each test condition for a weld penetration of 0.66 mm

Hot-tool temperature (°C)	Heating time (s)	Weld strength[a] (MPa)		Failure strain[b] (%)		Δl (mm)		Differential penetration $\Delta\eta$ ($\Delta\eta_T$) (10^{-2} mm)	
		δ_H = 0.25 mm	δ_H = 0.66 mm	δ_H = 0.25 mm	δ_H = 0.66 mm	δ_H = 0.25 mm	δ_H = 0.66 mm	δ_H = 0.25 mm	δ_H = 0.66 mm
230	10	42.4	—	2.08	—	0.70	—	6 (16)	—
230	10	30.9	—	1.44	—	0.75	—	6 (16)	—
230	10	30.9	—	1.46	—	0.65	—	11 (21)	—
245	10	60.6	42.2	3.98	2.15	0.81	0.99	−5 (5)	58 (68)
245	10	57.6	44.7	3.88	2.29	0.81	1.04	−5 (5)	53 (63)
245	10	58.5	46.9	3.88	2.39	0.80	1.05	−4 (6)	52 (62)
245	10	—	63.2	—	5.34	—	0.99	—	59 (69)
245	10	—	30.4	—	1.40	—	1.04	—	54 (64)
260	10	46.7	32.1	2.51	1.49	0.84	1.31	−8 (2)	27 (37)
260	10	52.1	65.2	3.08	—[c]	0.90	1.32	−14 (−4)	25 (35)
260	10	52.4	64.7	3.12	6.20[d]	0.88	1.40	−11 (−1)	18 (28)
260	10	—	65.0	—	5.95[d]	—	1.38	—	19 (29)
260	10	—	65.2	—	6.38[c]	—	1.36	—	22 (32)
275	10	—	66.3	—	6.45[c]	—	1.46	—	11 (23)
275	10	—	65.7	—	6.20[c]	—	1.42	—	15 (27)
275	10	—	65.0	—	6.20[d]	—	1.47	—	10 (22)
275	10	—	64.8	—	—[d]	—	1.51	—	7 (19)
275	10	—	65.1	—	—[d]	—	1.49	—	9 (21)
230	15	58.7	—	3.76	—	0.79	—	−3 (9)	—
230	15	39.3	—	2.00	—	0.91	—	−15 (−3)	—
230	15	50.1	—	2.81	—	0.79	—	−3 (9)	—
245	15	56.4	66.0	3.47	5.91	0.85	1.36	−9 (3)	22 (34)
245	15	50.8	65.2	2.98	5.96[c]	0.93	1.33	−17 (−5)	24 (36)
245	15	53.1	65.1	3.32	6.10[c]	0.85	1.36	−9 (3)	22 (34)
245	15	—	65.2	—	5.99[d]	—	1.43	—	15 (27)
245	15	—	65.1	—	6.01[c]	—	1.30	—	28 (40)
260	15	41.9	43.3	2.20	2.20	0.95	1.50	−19 (−5)	8 (22)
260	15	38.9	64.9	2.17	6.49[d]	0.98	1.47	−22 (−8)	10 (24)
260	15	40.6	65.2	2.08	6.01[c]	0.91	1.50	−15 (−1)	8 (22)
260	15	—	65.0	—	6.26[d]	—	1.51	—	7 (21)
260	15	—	45.8	—	2.37	—	1.52	—	5 (19)
275	15	—	66.6	—	6.03[c]	—	1.61	—	−4 (10)
275	15	—	65.3	—	6.37[c]	—	1.55	—	3 (17)
275	15	—	65.2	—	6.03[d]	—	1.59	—	−1 (13)
275	15	—	38.2	—	1.80	—	1.60	—	−2 (12)
275	15	—	31.5	—	1.46	—	1.59	—	−1 (13)
230	20	52.4	—	2.95	—	0.90	—	−14 (0)	—
230	20	48.0	—	2.61	—	0.89	—	−13 (1)	—
230	20	44.6	—	2.27	—	0.86	—	−10 (4)	—
245	20	46.6	66.2	2.37	6.05	0.95	1.55	−19 (−5)	3 (17)
245	20	45.9	65.0	2.51	5.88[c]	0.97	1.46	−20 (−6)	11 (25)
245	20	42.3	64.7	2.20	5.93[c]	0.93	1.46	−17 (−3)	11 (25)
245	20	—	65.0	—	6.16[d]	—	1.46	—	12 (26)
245	20	—	65.2	—	6.43[c]	—	1.42	—	15 (29)
260	20	39.2	28.2	1.95	1.29	0.89	1.66	−13 (3)	−9 (7)
260	20	35.2	65.0	1.86	6.03[c]	0.97	1.56	−20 (−4)	1 (17)
260	20	26.7	64.7	1.39	6.10[c]	0.93	1.57	−17 (−1)	0 (16)
260	20	—	65.3	—	6.31[c]	—	1.59	—	−2 (14)
260	20	—	24.4	—	1.08	—	1.63	—	−6 (10)
275	20	—	65.8	—	5.83[c]	—	1.73	—	−15 (1)
275	20	—	65.6	—	5.79[c]	—	1.63	—	−5 (11)
275	20	—	63.1	—	5.10	—	1.60	—	−3 (13)
275	20	—	27.9	—	1.29	—	1.62	—	−4 (12)
275	20	—	25.6	—	1.09	—	1.60	—	−3 (13)

[a] $\sigma_0 = 66.5$ MPa.
[b] $\varepsilon_0 = 7\%$.
[c] Specimen yielded at the weld before breaking at the weld.
[d] Specimen yielded outside the weld, necked and then broke at the weld.

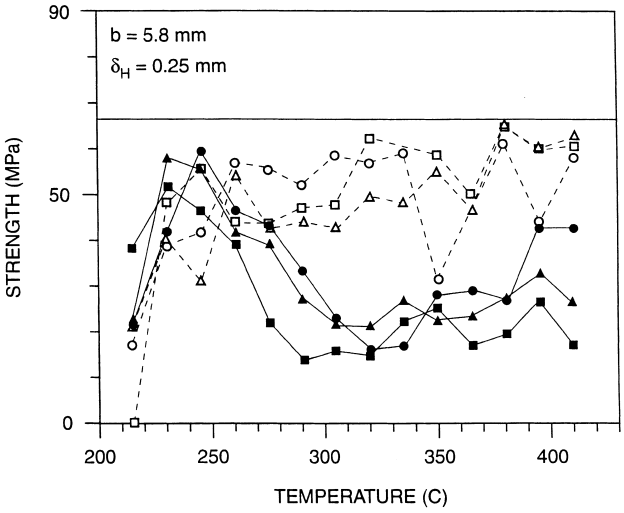

Fig. 11. Weld strength of 5.8-mm-thick undried (solid symbols) and dried (open symbols) PC as a function of the hot-tool temperature, with the heating time as parameter. Circles, triangles and squares correspond, respectively, to heating times of 10, 15, and 20 s. The melt and weld penetrations were maintained at 0.13 and 0.25 mm, respectively.

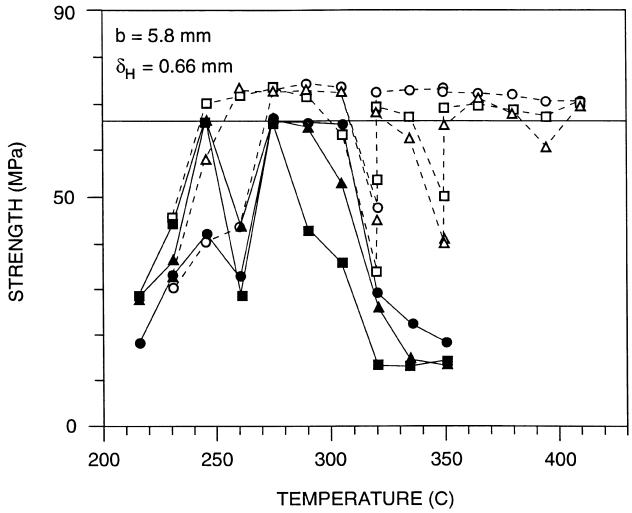

Fig. 12. Weld strength of 5.8-mm-thick undried (solid symbols) and dried (open symbols) PC as a function of the hot-tool temperature, with the heating time as parameter. Circles, triangles and squares correspond, respectively, to heating times of 10, 15, and 20 s. The melt and weld penetrations were maintained at 0.13 and 0.66 mm, respectively.

obtained from one test per test condition should only be used for determining general trends. The repeatability of weld strength data is explored in the next section.

Fig. 11 shows the weld strength (data from Table 5) of 5.8-mm-thick undried (solid symbols) and dried (open symbols) specimens for the lower weld penetration of 0.25 mm as a function the hot-tool temperature, for three heating times of 10, 15, and 20 s (indicated, respectively, by circles, triangles, and squares). The thin horizontal line represents the strength of the resin (66.5 MPa). The corresponding variation of the weld strength (data from Table 6) for the higher weld penetration of 0.66 mm is shown in Fig. 12. Thus, Figs. 11 and 12 compare the effect of the weld penetration (0.25 and 0.66 mm, respectively), other weld parameters being the same. Here again, for the same set of process conditions the dried material exhibits higher weld strengths, just as with 3-mm-thick specimens. For example, Fig. 11 shows that at the lower weld penetration (0.25 mm), the weld strength of the undried material is always lower than the strength of the material (maximum relative strength of 91%). In the undried material, relative weld strengths in the range of 88%–91% can be attained over a narrow process window of T_H = 230°C–245°C — the strength falls off at higher temperatures. In contrast, the strength of the dried material continues to increase from a relative strength of about 84% at T_H = 260°C to 95%–98% for T_H in the range of 380°C–410°C. Again, as with the 3-mm-thick specimens, higher strengths are attained at the higher weld penetration of 0.66 mm; Fig. 11 shows that 100% strength can be attained even in the undried material for T_H in the range of 245°C–290°C. Greater than 100% strengths can be obtained in the dried material for T_H in the range of 245°C–410°C. Thus, 5.8-mm-thick PC parts do not have to be dried before welding if the right hot-tool temperatures are used. A comparison of the weld failure strains in Tables 5 and 6 show that

1. at the smaller weld penetration (0.25 mm) welds in the dried material exhibit higher ductility, and
2. that the welds at the larger weld penetration (0.66 mm) exhibit very high ductility.

Again, as with the 3-mm-thick specimens, the very high relative weld strength in excess of 100% can be attributed to the increase in the cross-sectional area of the weld zone contributed by the flash. This effect should increase with the weld temperature — softer material undergoes more ''upsetting''.

Fig. 13 shows the fracture surfaces of 5.8-mm-thick undried and dried specimens that were welded at the lower weld penetration of 0.25 mm and a heating time of t_H = 10 s. The figures on the left (a, c) and right (b, d) correspond, respectively to undried and dried specimens. Fig. 13a and b corresponds to a hot-tool temperature of T_H = 245°C, at which (row 3 in Table 5) the undried material has a higher weld strength and failure strain (60.6 MPa, 3.98%) than the dried material (41.7 MPa, 1.98%) — the dried material appears to have a larger number of voids. Fig. 13c and d shows the fracture surface morphologies for T_H = 305°C, at which (row 7 in Table 5) the undried material has a much lower strength and ductility (22.9 MPa, 1.0%) than the dried material (59.1 MPa, 3.25%) — here the undried material has a large number of small voids, while the dried material has fewer but much larger voids.

The molten surfaces of 5.8-mm-thick, undried and dried specimens begin to exhibit some stringing at a hot-tool temperature of T_H = 275°C. Substantial stringing occurs at T_H = 295°C in the dried material (Fig. 4d–f). Both the undried and dried materials exhibit stringing for T_H in the

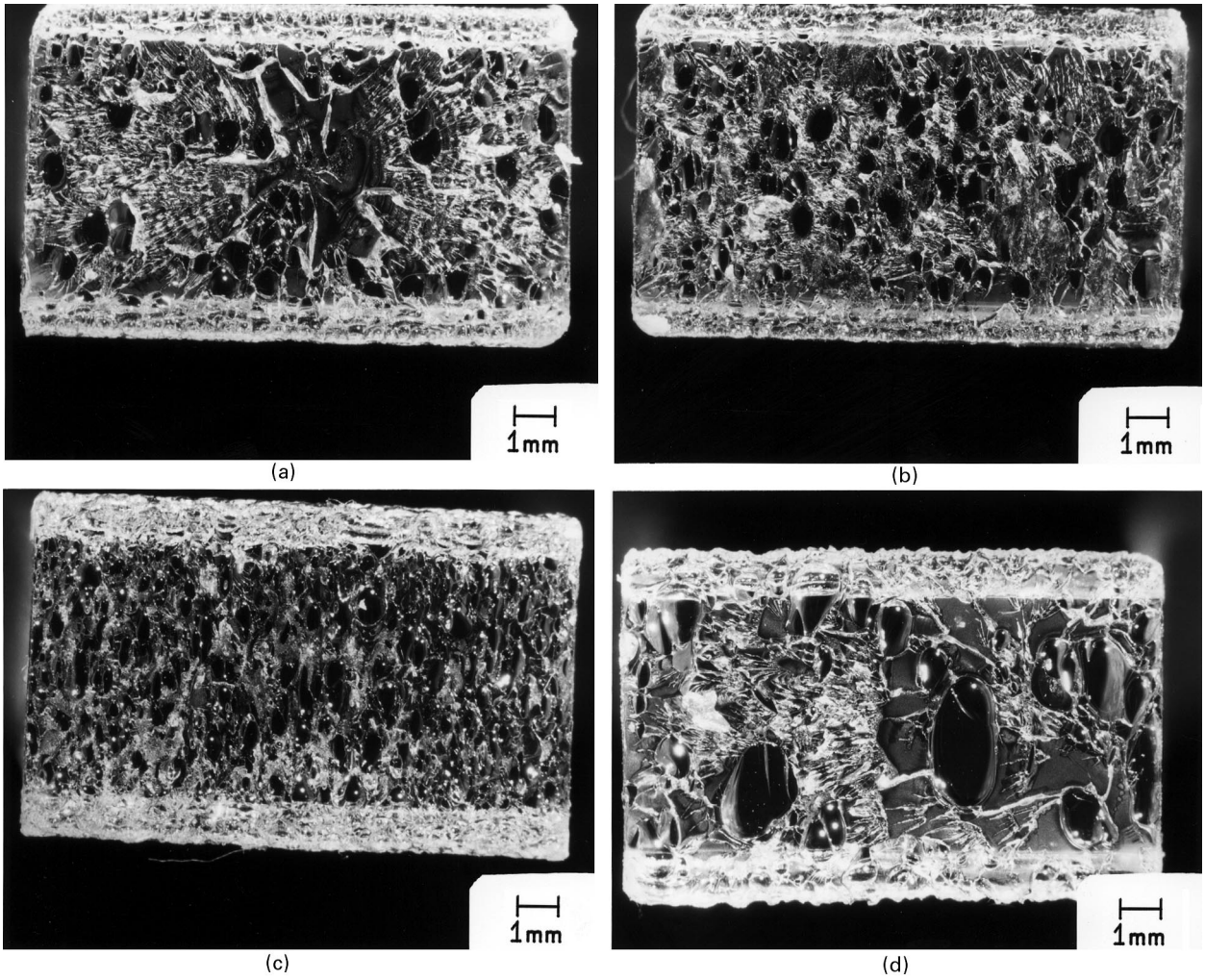

Fig. 13. Fracture surfaces of 5.8-mm-thick undried and dried PC specimens. The figures on the left (a, c) and right (b, d) correspond, respectively, to undried and dried specimens. The heating time was $t_H = 10$ s and the hot-tool temperatures were $T_H = 245$°C for (a) and (b) and $T_H = 305$°C for (c) and (d).

range of 305°C–365°C, with more stringing occurring in the dried material. However, the stringing in this range is less than in the range of 295°C–305°C. A perusal of the data in Table 5 (rows 6–9, 20–23, and 34–37) and Table 6 (rows 6–10, 23–27, and 41–46) shows that the dried material — which strings more — exhibits very high weld strengths for T_H in the range of 295°C–335°C. Thus, as in the 3-mm-thick specimens, stringing does not result in reduced weld strength. Again, in the undried material, the reduced weld strengths at higher weld temperatures correlates with increasing number of smaller bubbles — the dried material has a smaller number of larger bubbles.

For the smaller weld penetration of 0.25 mm, just as with the data for 3-mm-thick specimens (Table 3), the last two columns (Table 5) show mainly negative values of $\Delta\eta$. Although the corresponding values of $\Delta\eta_T$ are larger, they are still mostly negative. The same is also true of both $\Delta\eta$ and $\Delta\eta_T$ for the larger penetration of 0.66 mm (Table 6), although the values are larger than those for the smaller penetration. Also, just as for the 3-mm-thick specimens, in general, at any fixed heating time t_H, $\Delta\eta_T$ decreases with increases in the hot-tool temperature T_H and, for a fixed hot-tool temperature, $\Delta\eta_T$ again decreases with increases in the melt time.

5.2.1. Repeatability of test results

Fig. 11 (data from Table 5) shows sudden changes in the trend in strength variation with hot-tool temperature. For example, the strengths of the dried specimens at $T_H =$ 350°C and 395°C for $t_H = 10$ s, at $T_H = 245$°C and 365°C for $t_H = 15$ s, and at $T_H = 365$°C for $t_H = 20$ s show significant departures from the trends at neighboring temperatures. Fig. 12 (data from Table 6) shows similar departures from the trends in the dried material at $T_H = 320$°C and 350°C. This figure also shows a sudden change in the strengths of the undried material at $T_H = 260$°C. Clearly, the repeat data for the undried material at $T_H = 320$°C and 350°C show that this departure from the general trend is caused by scatter in the attainable weld strength. Since most of the data in this paper were obtained from one test for each condition, a

Table 8
Repeatability of strength and ductility for hot-tool welds of 5.8-mm-thick undried PC specimens as functions of the hot-tool temperature and the heating time. The weld and seal penetrations were maintained at 0.66 and 0.13 mm and the seal time was kept constant at 10 s. The averages and deviations are based on sets of five tests at each test condition (data from Table 7)

Hot-tool temperature (°C)	Heating time (s)	Weld strength[a] (MPa)		Failure strain[b] (%)		Δl (mm)		Average differential penetration $\Delta\eta$ ($\Delta\eta_T$) (10^{-2} mm)
		Average	Standard deviation	Average	Standard deviation	Average	Standard deviation	
245	10	45.5	11.8	2.71	1.52	1.02	0.03	55 (65)
260	10	58.4	14.7	5.01	2.35	1.35	0.04	22 (32)
275	10	65.4	0.6	6.29	0.12	1.47	0.03	10 (22)
245	15	65.3	0.4	5.99	0.07	1.35	0.05	22 (34)
260	15	56.9	11.2	4.67	2.18	1.50	0.02	7 (21)
275	15	53.4	17.1	4.34	2.48	1.59	0.02	−1 (13)
245	20	65.2	0.6	6.09	0.22	1.47	0.05	10 (24)
260	20	49.5	21.2	4.16	2.72	1.61	0.04	−3 (13)
275	20	49.6	20.9	3.82	2.42	1.64	0.05	−6 (10)

[a] $\sigma_0 = 66.5$ MPa.
[b] $\varepsilon_0 = 7\%$.

special set of repeat tests were done to assess the repeatability of the data.

To evaluate the repeatability of weld strength data, repeat tests were done on 5.8-mm-thick undried PC specimens at three heating times (10, 15, and 20 s) and two weld penetrations: At the lower weld penetration of 0.25 mm, three repeat tests were done at three hot-tool temperatures (230°C, 245°C, and 260°C); at the higher weld penetration

Table 9
Strength and ductility data for hot-tool welds of 5.8-mm-thick dried PC specimens, at a strain rate of $\dot{\varepsilon} = 0.01\ s^{-1}$, as functions of the hot-tool temperature and the seal and heating times. The melt and weld penetrations were maintained at 0.13 and 0.66 mm, respectively

Hot-tool temperature (°C)	Seal time (s)	Heating time (s)	Weld strength[a] (MPa)	Failure strain[b] (%)	Δl (mm)	Differential penetration $\Delta\eta$ ($\Delta\eta_T$) (10^{-2} mm)
275	5	10	72.5	5.42[c]	1.55	3 (15)
275	5	15	73.0	5.27[c]	1.68	−10 (4)
275	5	20	71.6	5.35[c]	1.71	−14 (2)
275	10	5	40.9	1.98	0.75	83 (91)
275	10	10	72.4	5.69[c]	1.55	3 (15)
275	10	15	72.6	4.83	1.54	4 (18)
275	10	20	73.1	5.25	1.69	−11 (5)
290	10	5	50.9	2.56	0.95	62 (70)
290	10	10	74.1	5.36	1.59	−1 (11)
290	10	15	72.8	5.46	1.69	−11 (3)
290	10	20	71.6	4.89	1.70	−13 (5)
305	10	5	46.0	2.34	1.18	39 (49)
305	10	10	72.8	5.93[c]	1.71	−14 (−2)
305	10	15	72.0	5.37[c]	1.75	−18 (−2)
305	10	20	62.9	3.59[c]	1.77	−19 (−1)
410	10	10	69.6	5.05[d]	1.91	−33 (−15)
410[d]	10	15	68.8	5.27[d]	1.85	−28 (−6)
410[d]	10	20	69.2	4.81[c]	1.93	−36 (−12)
410[d]	15	20	68.0	4.88[c]	1.88	−30 (−6)
410[d]	20	20	68.9	4.96[c]	1.89	−32 (−8)

[a] $\sigma_0 = 66.5$ MPa.
[b] $\varepsilon_0 = 7\%$.
[c] Specimen yielded at the weld before breaking at the weld.
[d] Specimen sagged immediately after the joining phase.

Table 10
Strength and ductility data for hot-tool welds of 12-mm-thick undried and dried PC specimens, at a strain rate of $\dot{\varepsilon} = 0.01\ s^{-1}$, as functions of the hot-tool temperature and the heating time. The melt and weld penetrations were maintained at 0.13 and 0.25 mm, respectively, and the seal time was kept constant at 10 s

Hot-tool temperature (°C)	Heating time (s)	Weld strength[a] (MPa)		Failure strain[b] (%)		Δl (mm)		Differential penetration $\Delta\eta$ ($\Delta\eta_T$) (10^{-2} mm)	
		Undried	Dried	Undried	Dried	Undried	Dried	Undried	Dried
230	10	19.1	28.4	0.78	1.14	0.28	0.32	48 (58)	44 (54)
245	10	56.9	39.7	2.92	1.88	0.58	0.44	18 (28)	32 (42)
260	10	56.7	63.2	3.23	3.91	0.20	0.56	30 (40)	20 (30)
275	10	58.6	64.8	3.42	—	0.58	0.75	18 (30)	1 (13)
290	10	55.6	53.2	2.66	2.94	0.77	0.79	−1 (11)	−3 (9)
305	10	24.0	50.4	0.98	2.87	0.89	0.86	−13 (−1)	−10 (2)
230	15	49.0	[c]	2.51	[c]	0.56	[c]	20 (32)	[c]
245	15	59.0	56.6	3.14	2.75	0.72	0.72	4 (16)	4 (16)
260	15	54.9	66.9	2.69	4.35	0.71	0.80	5 (19)	−4 (10)
275	15	55.4	56.0	3.18	3.37	0.85	0.86	−9 (5)	−10 (4)
290	15	29.6	49.6	1.41	2.75	0.81	0.85	−5 (9)	−9 (5)
305	15	24.0	42.2	—	2.22	0.88	0.89	−11 (5)	−13 (3)
230	20	47.2	[c]	2.23	[c]	0.72	[c]	4 (18)	[c]
245	20	58.5	60.3	3.31	3.56	0.83	0.77	−6 (8)	−1 (13)
260	20	53.9	57.4	2.65	2.79	0.80	0.77	−4 (12)	−1 (15)
275	20	41.0	43.4	2.02	1.96	0.83	0.91	−6 (10)	−15 (1)
290	20	23.6	35.4	1.05	1.81	0.88	0.81	−11 (7)	−5 (13)
305	20	22.1	37.1	1.05	1.70	0.90	1.01	−14 (4)	−25 (−7)

[a] $\sigma_0 = 66.5$ MPa.
[b] $\varepsilon_0 = 7\%$.
[c] Specimen did not weld.

of 0.66 mm, five repeat tests were done at three hot-tool temperatures (245°C, 260°C, and 275°C). The data for these tests are listed in Table 7.

Mean values and standard deviations for four weld parameters, for the sets of five repeat tests for a weld penetration of 0.66 mm, are listed in Table 8. The standard deviations in the weld strengths and failure strains are particularly small at $T_H = 245$°C for $t_H = 15$ and 20 s, and at $T_H = 275$°C for $t_H = 10$ s, being less than 1% of the means. Thus, repeatable weld strength and ductility can be expected at these weld conditions. Although very high weld strengths can also be achieved at the other listed conditions, the standard deviations are very large, varying from 20% to 40% of the mean strengths. Therefore, for a complete mapping of the optimum weld conditions, more repeat data are needed at each test condition. Note that the standard deviation in length changes is uniformly small and is insensitive to the hot-tool temperature and the heating time.

5.2.2. Effect of seal time

For 5.8-mm-thick dried PC specimens, Table 9 lists data for a small number of weld tests in which the seal time was varied from 5 to 20 s. (All other data in this paper are for a fixed seal time of 10 s.) At $T_H = 275$°C, very high weld strengths with excellent ductility can be obtained at a seal time of 5 s, and the strength and ductility are not very sensitive to the heating time being varied from 10 to 20 s. Comparable strengths can be attained for a seal time of 10 s, although the ductility appears to be a little lower. The three data sets for $T_H = 275$°C, 290°C, and 305°C show that the strengths and ductilities for a heating time of 5 s are low. The last three rows in this table show that the seal time (10, 15, 20 s) has a very small effect on the strength and ductility for a heating time of 20 s.

The last column in Table 9 shows that both $\Delta\eta$ and $\Delta\eta_T$ exhibit the same trends as the 3- and 5.8-mm-thick specimens. In general, at any fixed heating time t_H, $\Delta\eta_T$ decreases with increases in the hot-tool temperature T_H and, for a fixed hot-tool temperature, $\Delta\eta_T$ again decreases with increases in the melt time.

5.3. 12-mm-thick specimens

Strength and ductility data for 12-mm-thick undried and dried PC specimens as functions of the hot-tool temperature and the heating time are listed in Tables 10 and 11 for weld penetrations of 0.25 and 0.66 mm, respectively. The PC specimens had a yield strength of 66.5 MPa, higher than that of the 3-mm-thick specimens, and a yield strain of 7%. The melt penetration was maintained at 0.13 mm and the seal time was kept constant at 10 s. The hot-tool temperature was varied between 230°C and 410°C. Here again, the weld strength data in Tables 10 and 11 were obtained from one test per test condition studied.

Table 11
Strength and ductility data for hot-tool welds of 12-mm-thick undried and dried PC specimens, at a strain rate of $\dot{\varepsilon} = 0.01\ s^{-1}$, as functions of the hot-tool temperature and the heating time. The melt and weld penetrations were maintained at 0.13 and 0.66 mm, respectively, and the seal time was kept constant at 10 s

Hot-tool temperature (°C)	Heating time (s)	Weld strength[a] (MPa)		Failure strain[b] (%)		Δl (mm)		Differential penetration $\Delta\eta$ ($\Delta\eta_T$) (10^{-2} mm)	
		Undried	Dried	Undried	Dried	Undried	Dried	Undried	Dried
245	10	53.2	36.9	2.81	1.71[c]	0.53	0.43	104 (114)	114 (124)
260	10	66.2	47.7	5.10	2.17	0.69	0.75	89 (99)	83 (93)
275	10	62.8	69.9	4.03	4.37	0.98	1.10	60 (72)	47 (59)
290	10	48.1	71.4	2.34	4.91	1.00	1.24	57 (69)	33 (45)
305	10	32.9	73.9	1.46[d]	5.47	1.21	1.56	37 (49)	1 (13)
320	10	21.5	74.2	0.90[d]	5.44[e]	1.46	1.57	11 (25)	0 (14)
335	10	20.8	54.6	0.88[d]	2.69[d]	1.55	1.60	3 (17)	−3 (11)
350	10	—	73.4	—	5.62[e]	—	1.75	—	−18 (−4)
365	10	—	73.5	—	—[e]	—	1.79	—	−22 (−6)
380	10	—	71.1	—	5.05	—	1.75	—	−18 (−2)
395	10	—	65.5	—	3.74[d]	—	1.74	—	−17 (−1)
410	10	—	72.8	—	4.96[e]	—	1.71	—	−14 (4)
245	15	66.3	[f]	4.98	[f]	0.74	[f]	84 (96)	[f]
260	15	66.5	70.9	5.37	4.69	0.98	1.02	60 (74)	56 (60)
275	15	67.2	72.8	5.42	5.15[e]	1.35	1.42	23 (37)	15 (29)
290	15	27.5	73.0	1.20[d]	5.08[e]	1.41	1.61	17 (31)	−4 (10)
305	15	24.8	69.9	1.05[d]	4.37	1.52	1.73	5 (21)	−15 (1)
320	15	12.1	68.5	0.46[d]	4.30	1.64	1.70	−6 (10)	−13 (3)
335	15	13.3	42.7	0.54[d]	1.93[d]	1.65	1.70	−8 (10)	−13 (5)
350	15	—	71.6	—	4.61	—	1.79	—	−22 (−4)
365	15	—	61.2	—	3.32	—	1.75	—	−18 (2)
380	15	—	62.6	—	3.30	—	1.75	—	−18 (2)
395	15	—	54.9	—	2.73[d]	—	1.74	—	−17 (3)
410	15	—	49.8	—	2.42[d]	—	1.78	—	−20 (2)
245	20	67.3	42.5	5.57	2.12[c]	0.97	1.04	61 (75)	53 (67)
260	20	67.7	72.3	—	5.10[e]	1.31	1.36	27 (43)	22 (38)
275	20	68.2	72.6	6.10[e]	5.42[e]	1.57	1.68	0 (16)	−10 (6)
290	20	22.2	72.1	0.88[d]	4.81	1.56	1.69	1 (19)	−11 (7)
305	20	15.1	64.9	0.66[d]	3.61	1.66	1.78	−9 (9)	−20 (−2)
320	20	12.1	55.4	0.46[d]	2.81	1.61	1.69	−4 (14)	−11 (7)
335	20	12.7	37.9	0.51[d]	1.64[d]	1.77	1.78	−19 (1)	−20 (0)
350	20	—	54.8	—	2.56	—	1.83	—	−25 (−3)
365	20	—	44.2	—	2.03	—	1.79	—	−22 (0)
380	20	—	62.5	—	3.49	—	1.82	—	−24 (−2)
395	20	—	44.1	—	2.00[d]	—	1.75	—	−18 (6)
410	20	—	47.9	—	2.39[d]	—	1.80	—	−20 (4)

[a] $\sigma_0 = 66.5$ MPa.
[b] $\varepsilon_0 = 7\%$.
[c] Specimen had debris on weld surface.
[d] Weld surface had white parallel streaks.
[e] Specimen yielded at the weld before breaking at the weld.
[f] Specimen did not weld.

Fig. 14 shows the weld strength (data from Table 10) of 12-mm-thick undried (solid symbols) and dried (open symbols) specimens for the smaller weld penetration of 0.25 mm, as a function the hot-tool temperature, for three heating times of 10, 15, and 20 s (indicated, respectively, by circles, triangles, and squares). The thin horizontal line represents the strength of the resin (66.5 MPa). The corresponding variation of the weld strength (data from Table 11) for the higher weld penetration of 0.66 mm is shown in Fig. 15. Figs. 14 and 15 compare the effect of the weld penetration (0.25 and 0.66 mm, respectively), for the same weld parameters. For the same set of process conditions, higher weld strengths in the 12-mm-thick specimens are obtained in the dried material — just as with the other two thicknesses (3 and 5.8 mm). At the smaller weld penetration of 0.25 mm, relative weld strengths of about 88% can be attained in the undried material over a narrow process window of $T_H = 245°C–275°C$ — the strength falls off at

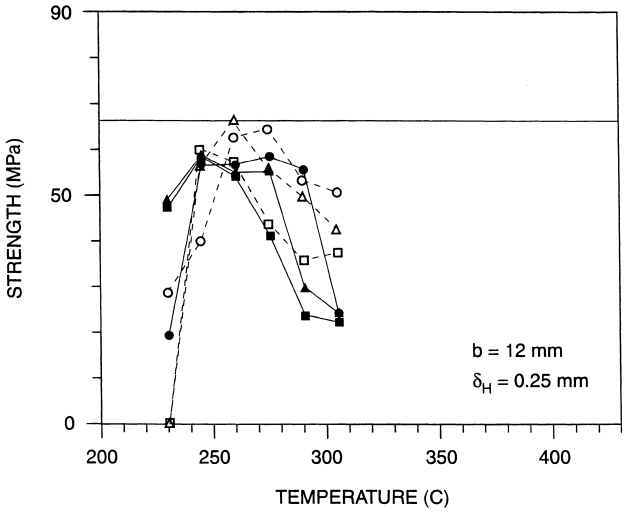

Fig. 14. Weld strength of 12-mm-thick undried (solid symbols) and dried (open symbols) PC as a function of the hot-tool temperature, with the heating time as parameter. Circles, triangles and squares correspond, respectively, to heating times of 5, 10, and 20 s. The melt and weld penetrations were maintained at 0.13 and 0.25 mm, respectively.

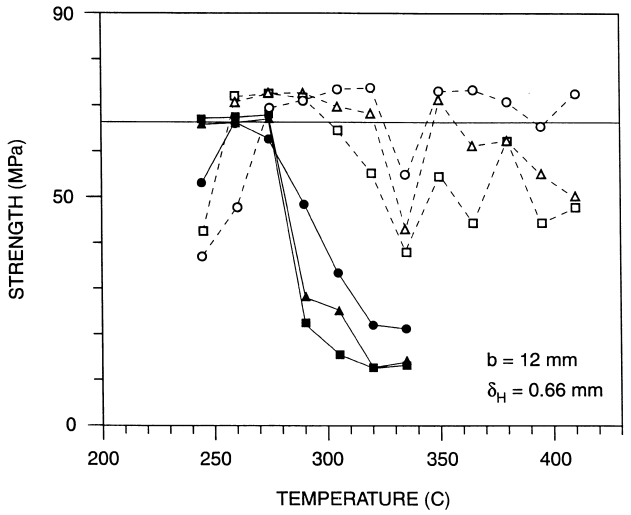

Fig. 15. Weld strength of 12-mm-thick undried (solid symbols) and dried (open symbols) PC as a function of the hot-tool temperature, with the heating time as parameter. Circles, triangles and squares correspond, respectively, to heating times of 10, 15, and 20 s. The melt and weld penetrations were maintained at 0.13 and 0.66 mm, respectively.

higher temperatures. In the dried material, higher relative weld strengths in the range of 87%–100% can be obtained over the same temperature range. Again, the strength falls off at higher temperatures. At this weld penetration the weld failure strains are relatively small. At the larger weld penetration of 0.66 mm, 100% relative weld strength can be obtained in the undried material over a narrow temperature range of $T_H = 245°C–275°C$; the strength drops off rapidly at higher temperatures. In the dried material, apparent strengths in excess of 100% are obtainable over a wide temperature range ($T_H = 260°C–410°C$). The welds are more ductile, especially in the dried material.

Again, as with 3- and 5.8-mm-thick specimens, the last two columns in Tables 10 and 11 show that, in general, at any fixed heating time t_H, $\Delta\eta_T$ decreases with increases in the hot-tool temperature T_H and, for a fixed hot-tool temperature, $\Delta\eta_T$ decreases with increases in the melt time. A comparison of the last two columns in Tables 4–7, 11, and 12 show a general trend in which — for any fixed hot-tool temperature, weld penetration, and melt time — both $\Delta\eta$ and $\Delta\eta_T$ increase with the specimen thickness. This is to be expected, because, for the same weld pressure, the molten film will be squeezed outward more slowly with increasing specimen thickness, so that this effect and solidification will result in larger $\Delta\eta$ and $\Delta\eta_T$.

Fig. 16 shows the fracture surfaces of 12-mm-thick undried and dried specimens that were welded at the lower weld penetration of 0.25 mm and a heating time of $t_H = 10$ s. The figures on the left (a, c) and right (b, d) correspond, respectively to undried and dried specimens. Fig. 16a and b corresponds to a hot-tool temperature of $T_H = 275°C$, at which (row 4 in Table 10) the undried material has a slightly lower weld strength (58.6 MPa) than the dried material (64.8 MPa) — the dried material appears to have fewer but larger voids. Fig. 16c and d shows the fracture surface morphologies for $T_H = 305°C$, at which (row 6 in Table 10) the undried material has a much lower strength (24.0 MPa) and ductility (failure strain of 0.98%) than the dried material (50.4 MPa and 2.87%). Here the undried material has a very large number of small voids, while the dried material has fewer but larger voids. The morphologies in these four figures seem to indicate that a larger number of small voids reduces the weld strength more than does a smaller number of larger ones.

Fig. 17 shows the fracture surfaces of 12-mm-thick undried and dried specimens that were welded at the higher weld penetration of 0.66 mm and a longer heating time of $t_H = 15$ s; the hot-tool temperatures were the same as those for the specimens shown in Fig. 16. Fig. 17a and b corresponds to a hot-tool temperature of $T_H = 275°C$, at which (row 15 in Table 11) the undried material has a slightly lower weld strength (67.2 MPa) than the dried material (72.8 MPa) while the corresponding ductilities (failure strains of 5.42% and 5.15%) are quite high. Although the surface morphologies are similar, the dried material appears to have fewer but larger voids. In both these specimens, fast fracture appears to have initiated at voids, that are in a state of high triaxial stress, after substantial ductile void growth. Fig. 17c and d shows the fracture surface morphologies for $T_H = 305°C$, at which (row 17 in Table 11) the undried material has a much lower strength (24.8 MPa) and ductility (failure strain of 1.05%) than the dried material (69.9 MPa, 4.37%). Again, the undried material has a large number of small voids, while the dried material has fewer but larger voids. However, while the mechanism of failure for the dried material appears to be the same (Fig. 17b, d) at the two hot-tool temperatures, the mechanism of failure in the undried material appears to be totally different at the

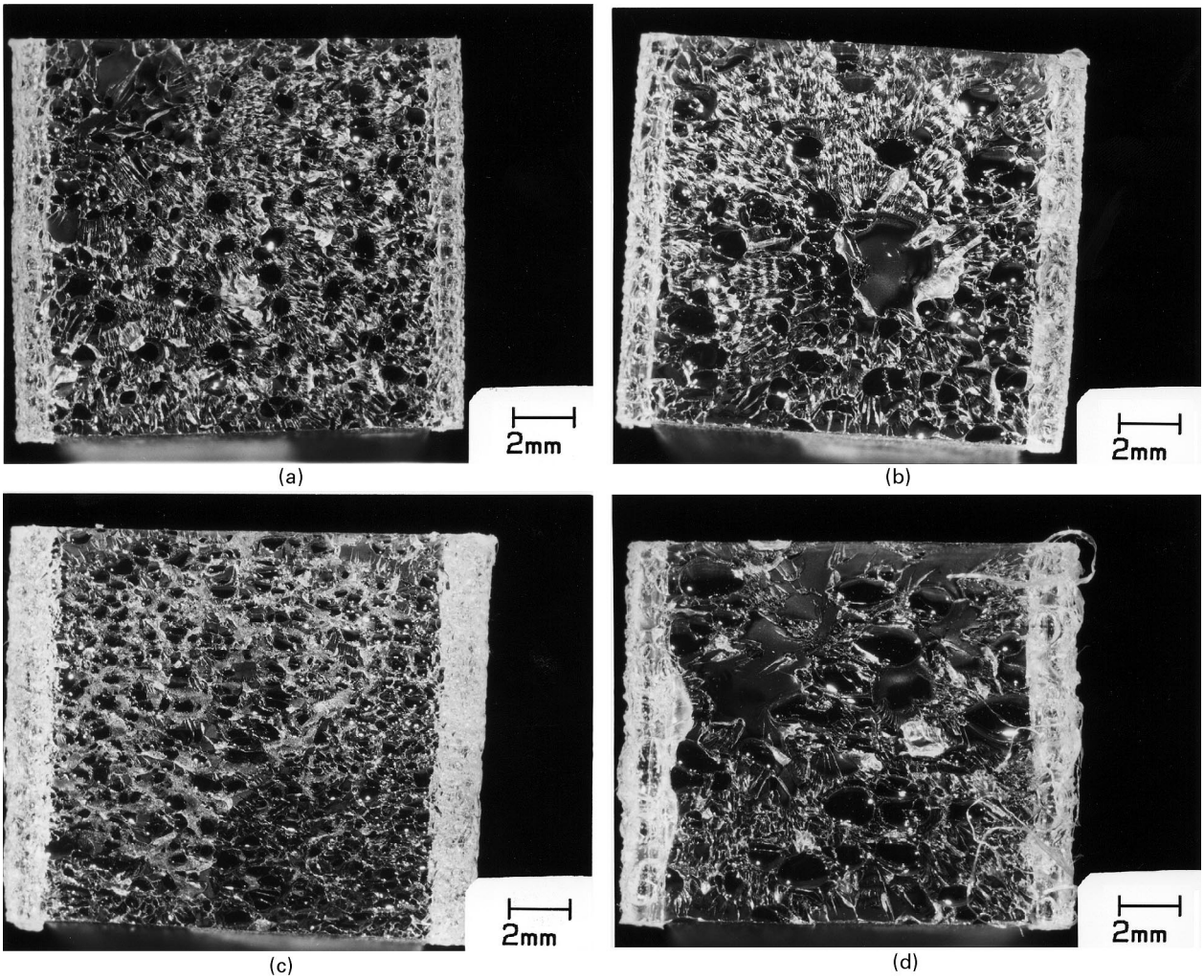

Fig. 16. Fracture surfaces of 12-mm-thick undried and dried PC specimens. The figures on the left (a, c) and right (b, d) correspond, respectively, to undried and dried specimens. The heating time was $t_H = 10$ s and the melt penetration was 0.25 mm. The hot-tool temperatures were $T_H = 275$°C for (a) and (b) and $T_H = 305$°C for (c) and (d).

higher temperature, as evidenced by the parallel white streaks. Each of the three strong welds (Fig. 17a, b, and d) appears to have failed by the same mechanism — ductile void growth followed by fast fracture. A comparison of Figs. 16 and 17 shows that the wider flash evident in Fig. 17 is consistent with the weld penetration being larger.

A perusal of the data in Table 10 (rows 4–6, 10–12, and 16–18) and Table 11 (rows 4–7, 16–19, and 28–31), corresponding to hot-tool temperatures in the range of 275°C–335°C, shows that the dried material — which strings more — exhibits very high weld strengths for T_H in the range of 295°C–335°C. Thus, as with 3- and 5.8-mm-thick specimens, stringing does not result in reduced weld strength. This finding contradicts the recommendations in Ref. [12]. In the undried material, reduced weld strengths at higher weld temperatures correlate with increasing number of smaller bubbles.

Table 12 lists strength and ductility data for 12-mm-thick dried PC specimens for a relatively large melt penetration of $\delta_0 = 0.38$ mm and a weld penetration of $\delta_H = 0.25$ mm for T_H in the range of 260°C–305°C. The strengths and ductilities are comparable but somewhat higher for the same weld penetration but a lower melt penetration of 0.13 mm (Table 10). However, much higher strengths and ductilities are obtained at $\delta_0 = 0.13$ mm and $\delta_H = 0.66$ mm (Table 11).

5.4. Dual hot-tool temperatures

The use of high hot-tool temperatures could cause ‘‘read-through’’ (visible surface distortion on an appearance surface of a part caused by residual stresses in the weld), resulting in poor surface appearance — especially in thin-walled parts. Just lowering the welding temperature may not help because adequate weld strengths may not be attainable at the low temperature at which no read-through occurs. One way of reducing read-through could be to use a lower temperature on the thinner appearance part of the assembly and a higher temperature on the other, non-appearance part.

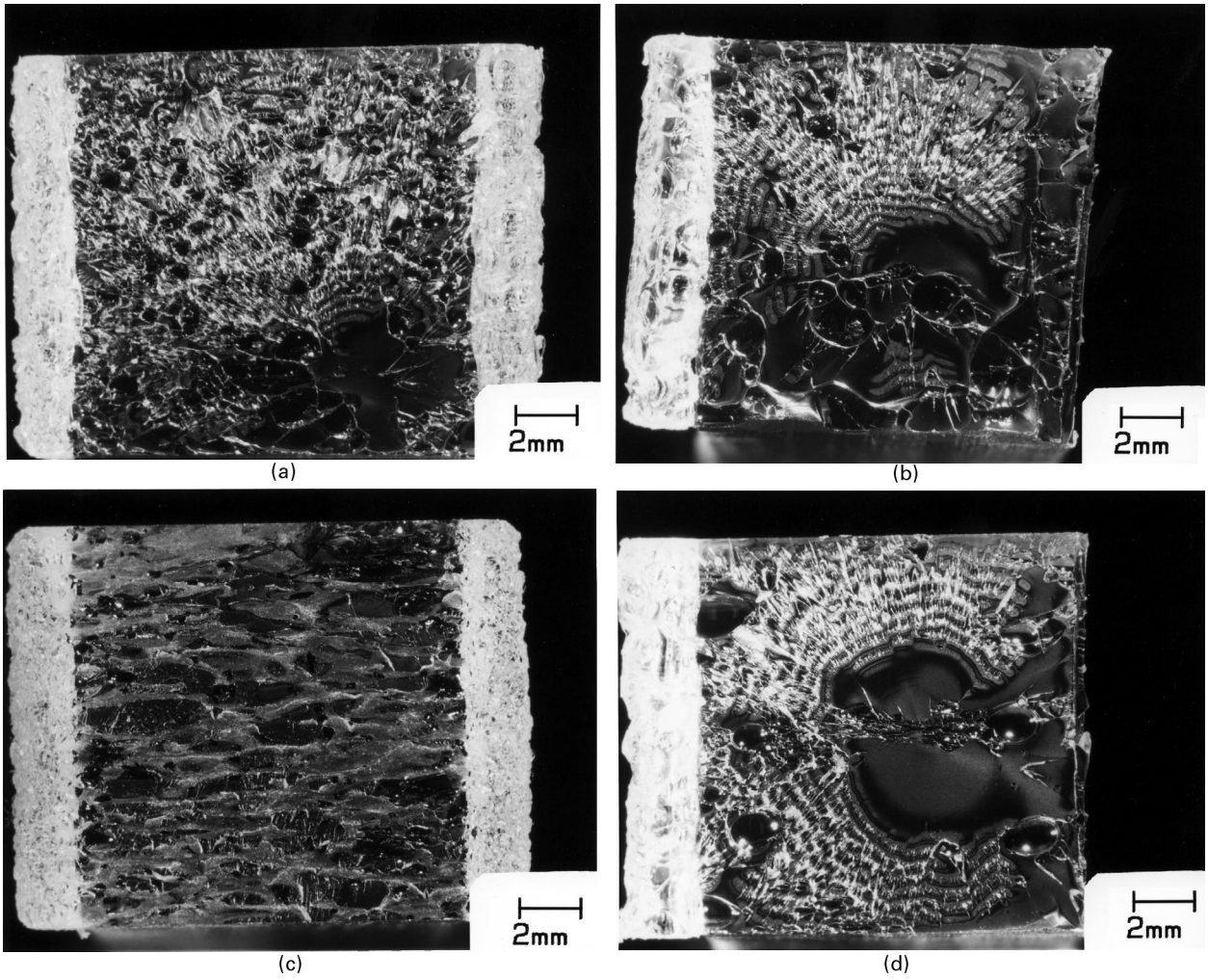

Fig. 17. Fracture surfaces of 12-mm-thick undried and dried PC specimens. The figures on the left (a, c) and right (b, d) correspond, respectively, to undried and dried specimens. The heating time was $t_H = 15$ s and the melt penetration was 0.66 mm. The hot-tool temperatures were $T_H = 275$°C for (a) and (b) and $T_H = 305$°C for (c) and (d).

To explore this approach, dual temperature tests were done on undried and dried 5.8-mm-thick specimens at fixed melt and weld penetrations of 0.13 and 0.25 mm, respectively. Two lower temperatures of 200°C and 215°C, and three high-side temperatures of 230°C, 245°C, and 260°C were tried. The heating times were 10, 15, 20, and 30 s with a seal time of 10 s. A seal time of 20 s was also tried at the 30-s heating time. The weld strength data for these tests are listed in Table 13. For comparison with single temperature welding, the last three rows in this table list the weld strength data (from Table 5) for a weld temperature of 215°C.

For the undried material, the data in the last three rows show a maximum weld strength of 38.3 MPa (58.6% relative weld strength) and a failure strain of 1.83%, corresponding to a weld temperature of 215°C. For the dual temperature case, the highest strength of 40.9 MPa (61.5% relative strength), with a relatively high failure strain of 2.41%, was attained (row 18) with low- and high-side hot-tool temperatures of 215°C and 245°C. For this temperature combination, the weld strengths are equivalent or slightly higher than those for the 215°C/215°C combination for equivalent process conditions. The 215°C/230°C combination gives better strengths. A 200°C/230°C combination gives a maximum strength (row 4) of 21.8 MPa (32.8% relative strength) and a failure strain of 1.08% for a seal time of 10 s. An increased seal time of 20 s results in an increase in the weld strength to 23.5 MPa (35.3% relative strength) and a failure strain of 1.21%. These results do show that increases in temperature do give better strengths. For example, the 200°C/230°C combination gives lower strengths than the 215°C/230°C combination. Similarly, the 215°C/230°C combination gives lower strengths than the 215°C/245°C combination. This trend also applies to failure strains.

In the dried material, a 215°C/260°C combination gives a maximum strength of 40.9 MPa (61.5% relative strength) and a failure strain of 1.98%, compared to a maximum of 21.1 MPa for the 215°C/215°C combination. The 200°C/260°C combination results in lower strengths. Here, again,

Table 12
Strength and ductility data for hot-tool welds of 12-mm-thick dried PC specimens, at a strain rate of $\dot{\varepsilon} = 0.01 s^{-1}$, as functions of the hot-tool temperature and the heating time. The melt and weld penetrations were maintained at 0.38 and 0.25 mm, respectively, and the seal time was kept constant at 10 s

Hot-tool temperature (°C)	Heating time (s)	Weld strength[a] (MPa)	Failure strain[b] (%)	Δl (mm)	Differential penetration $\Delta\eta$ ($\Delta\eta_T$) (10^{-2} mm)
260	10	53.0	2.90	1.28	−1 (9)
275	10	65.1	3.60	1.68	−41 (−29)
290	10	63.1	3.82	1.74	−47 (−35)
305	10	38.6	1.78	1.75	−48 (−36)
260	15	62.2	3.78	1.61	−34 (−20)
275	15	51.6	2.46	1.83	−56 (−42)
290	15	52.5	2.68	1.75	−48 (−34)
305	15	29.2	1.44	1.79	−52 (−36)
260	20	55.8	2.95	1.63	−36 (−20)
275	20	46.6	2.68	1.85	−58 (−42)
290	20	35.6	1.58	1.87	−60 (−42)
305	20	31.6	1.53	1.69	−42 (−24)

[a] $\sigma_0 = 66.5$ MPa.
[b] $\varepsilon_0 = 7\%$.

the 200°C/260°C combination results in lower strengths and failure strains in comparison to the 215°C/260°C combination. Although data comparing undried and dried materials at the same process conditions are not available, the results in this section suggest that a dual temperature strategy may help in reducing weld read-through problems.

6. Concluding remarks

It has been shown that high strengths can be attained in hot-tool welds of both undried and dried polycarbonate specimens. However, the hot-tool temperature window for attaining high weld strengths is very wide for dried specimens but quite narrow for the undried specimens. The thickness of the part does have a small effect — with increasing part thickness, the optimum temperature process window appears to shift to higher temperatures. A higher weld penetration appears to result in a higher weld strength. An increase in the heating time appears to reduce the hot-tool temperature required for obtaining high weld strengths.

Within the weld parameters studied, in the undried material the highest weld strengths, equal to that of the base material, are obtained at the following conditions: at (T_H = 260°C–290°C, t_H = 10 s), (T_H = 245°C–290°C, t_H = 15 s), and (T_H = 230°C–275°C, t_H = 20 s) for 3-mm-thick specimens; (T_H = 275°C–305°C, t_H = 10 s), (T_H = 275°C–290°C, t_H = 15 s), and (T_H = 245°C, t_H = 20 s) for 5.8-mm-thick specimens; and (T_H = 260°C–275°C, t_H = 10 s) and (T_H = 245°C–275°C, t_H = 15 and 20 s) for 12-mm-thick specimens. Based on repeat tests, consistently high weld strengths were demonstrated in 5.8-mm-thick specimens at (T_H = 275°C, t_H = 10 s) and (T_H = 245°C, t_H = 15 and 20 s).

Stringing is not responsible for reduced weld strengths. In the dried material, which strings more, very high strengths are obtained in the temperature range of T_H = 275°C–305°C, the temperature range in which the highest amount of stringing was observed. In the undried material, with increase in the hot-tool temperature, it is the increase in the number of small bubbles that results in reduced strength. The dried material has fewer but larger bubbles.

One interesting result is that very high weld strengths, equal to that of the base material, can be obtained in the presence of bubbles in the weld zone. A small number of large bubbles do not have much effect. However, a large number of small bubbles do result in reduced strength. Whether this reduction is caused just by the large number of bubbles in the weld plane or by layers of bubbles perpendicular to the weld plane has not been estabilished.

It has been shown that by using dual hot-tool temperatures for the two specimens being welded, substantial weld strengths can be achieved even when one surface is heated to a lower temperature than at which adequate strengths can be attained by heating the two surfaces to the same temperature. This dual temperature strategy may help in reducing weld read-through problems.

Most of the data in this paper were obtained from one test per weld process condition studied. While such data do not provide information on repeatability, they are useful for an initial mapping of weldability over a wide range of weld process conditions. Strength data as a function of the hot-tool temperature show unexplained breaks from general trends. Repeatability studies show that while high weld strengths can be obtained over a wide process window, repeatable high strengths are only achievable over a narrower process window. The large variability in the data is most likely caused by deposits on the hot-tool surface and by variations in the topography of the molten surfaces at the beginning of the joining phase. While hot-tool welding can produce strong welds, it requires careful dimensional and

Table 13
Strength and ductility data for dual temperature hot-tool welds of 5.8-mm-thick undried and dried PC specimens, at a strain rate of $\dot{\varepsilon} = 0.01\ s^{-1}$, as functions of the hot-tool temperature and the heating time. The melt and weld penetrations were maintained at 0.13 and 0.25 mm, respectively, and the seal time was kept constant at 10 s

Hot-tool temperature (°C)		Heating time (s)	Seal time (s)	Weld strength[a] (MPa)		Failure strain[b] (%)		Δl (mm)		Differential penetration $\Delta\eta$ ($\Delta\eta_T$) (10^{-2} mm)	
Right	Left			Undried	Dried	Undried	Dried	Undried	Dried	Undried	Dried
200	230	10	10	14.1	—	0.62	—	0.93	—	−17 (−8)	—
200	230	15	10	19.6	—	0.98	—	1.37	—	−61 (−50)	—
200	230	20	10	20.1	—	1.00	—	1.52	—	−76 (−63)	—
200	230	30	10	21.8	—	1.08	—	1.64	—	−88 (−73)	—
200	230	30	20	23.5	—	1.21	—	1.63	—	−86 (−71)	—
200	260	10	10	—	13.0	—	0.57	—	1.04	—	−28 (−19)
200	260	15	10	—	28.4	—	1.31	—	1.42	—	−66 (−54)
200	260	20	10	—	29.2	—	1.33	—	1.59	—	−83 (−69)
200	260	30	10	—	23.8	—	1.07	—	1.69	—	−93 (−77)
200	260	30	20	—	22.5	—	1.02	—	1.69	—	−93 (−77)
215	230	10	10	14.9	—	0.65	—	1.33	—	−57 (−48)	—
215	230	15	10	32.2	—	1.59	—	1.51	—	−75 (−64)	—
215	230	20	10	29.3	—	1.46	—	1.63	—	−86 (−73)	—
215	230	30	10	31.7	—	1.65	—	1.63	—	−86 (−70)	—
215	230	30	20	35.4	—	1.70	—	1.61	—	−85 (−69)	—
215	245	10	10	18.4	—	0.82	—	1.45	—	−69 (−60)	—
215	245	15	10	35.6	—	1.81	—	1.55	—	−79 (−68)	—
215	245	20	10	40.9	—	2.41	—	1.61	—	−85 (−72)	—
215	245	30	10	40.6	—	2.14	—	1.70	—	−94 (−77)	—
215	245	30	20	37.7	—	2.13	—	1.66	—	−90 (−73)	—
215	260	10	10	—	28.6	—	1.35	—	1.37	—	−61 (−52)
215	260	15	10	—	40.9	—	1.98	—	1.64	—	−88 (−76)
215	260	20	10	—	30.4	—	1.38	—	1.66	—	−90 (−76)
215	260	30	10	—	38.1	—	1.81	—	1.75	—	−100 (−83)
215	260	30	20	—	28.5	—	1.30	—	1.83	—	−107 (−90)
215	215	10	10	21.9	17.2	0.98	0.81	0.38	0.36	38 (46)	40 (48)
215	215	15	10	22.9	21.1	1.03	0.95	0.65	0.64	11 (21)	13 (23)
215	215	20	10	38.3	[c]	1.83	[c]	0.79	[c]	−3 (9)	[c]

[a] $\sigma_0 = 66.5$ MPa.
[b] $\varepsilon_0 = 7\%$.
[c] Specimen did not weld.

hot-tool temperature control, and a continuous cleaning of the hot-tool surface. In contrast, it is much easier to control the weld processing conditions in the vibration welding process.

Careful measurements of the differences between the initial and final lengths of specimens have not completely been reconciled with the differences expected on the basis of the machine stop settings. This discrepancy may either result from inaccuracies in the machine or from an inadequate analysis of thermal expansion effects. The length change data in this paper provide information for a more careful analysis of this welding process. The apparent variability of this welding process points to the need for more data at each test condition for a better mapping of the optimum welding conditions.

Acknowledgements

This work was supported by GE Plastics and the NIST ATP Project: Engineering Design with Injection-Molded Thermoplastics. The contributions of K.R. Conway, who carried out all the tests, and the inputs of L.P. Inzinna are greatly appreciated.

References

[1] Stokes VK. Polym Eng Sci 1989;29:1310.
[2] Potente H. Natrop J. Polym Eng Sci 1989;29:1649.
[3] Barber P, Atkinson JR. J Mater Sci 1972;7:1131.
[4] Barber P, Atkinson JR. J Mater Sci 1974;9:1456.
[5] Bucknall CB, Drinkwater IC, Smith GR. Polym Eng Sci 1980;20:432.

[6] Egen U, Ehrenstein GW. DVS Berichte 1983;84:49.
[7] Andrews JRF, Bevis M. J Mater Sci 1984;19:645.
[8] Andrews JRF, Bevis M. J Mater Sci 1984;19:653.
[9] Watson MN, Murch MG. Polym Eng Sci 1989;29:1382.
[10] Gehde M, Bevan L, Ehrenstein GW. Polym Eng Sci 1992;32:586.
[11] Bowman J, Haunton J, Folkes MJ. SPE ANTEC Tech Papers 1990;36:1793.
[12] Nonhof CJ. Polym Eng Sci 1996;36:1184.
[13] Potente H. Kunststoffe 1977;67:17.
[14] Potente H. DVS Berichte 1983;84:41.
[15] Potente H, Tappe P. Polym Eng Sci 1989;29:1642.
[16] Pimputkar SM. Polym Eng Sci 1989;29:1387.
[17] Poslinski AJ, Stokes VK. Polym Eng Sci 1992;32:1147.
[18] Poslinski AJ, Stokes VK. SPE ANTEC Tech Papers 1992;38:1228.
[19] Gabler K, Potente H. J. Adhesion 1980;11:145.
[20] Potente H, Gabler K. Plastverarbiter 1980;31:203.
[21] El Barbari N, Michel J, Menges G. Kunststoffe 1986;76:20.
[22] El Barbari N, Michel J, Menges G. Kunststoffberater 1986;31:63.
[23] Muschik H, Radax M, Dragaun H, Eichinger F. Kunststoffe 1986;76:23.
[24] Stokes VK. Polymer 1998;39:2469.
[25] Carslaw HS, Jaeger JC. Conduction of heat in solids. Oxford: Oxford University Press, 1959.
[26] Stokes VK. Polym Eng Sci 1997;37:692.